Last Interglacial climate and sea-level evolution from a coupled ice sheet-climate model

Heiko Goelzer[1,a], Philippe Huybrechts[1], Marie-France Loutre[2], Thierry Fichefet[2]

[1]Earth System Sciences & Departement Geografie, Vrije Universiteit Brussel, Brussels, Belgium

[2]Université catholique de Louvain, Earth and Life Institute, Georges Lemaître Centre for Earth and Climate Research (TECLIM), Louvain-la-Neuve, Belgium.

[a]now at: Institute for Marine and Atmospheric Research, Utrecht University, Utrecht, the Netherlands

Correspondence to: H. Goelzer (h.goelzer@uu.nl, heiko.goelzer@vub.ac.be)

1 Abstract

As the most recent warm period in Earth's history with a sea-level stand higher than present, the Last Interglacial (~130 to 115 kyr BP) is often considered a prime example to study the impact of a warmer climate on the two polar ice sheets remaining today. Here we simulate the Last Interglacial climate, ice sheet and sea-level evolution with the Earth system model of intermediate complexity LOVECLIM v.1.3, which includes dynamic and fully coupled components representing the atmosphere, the ocean and sea ice, the terrestrial biosphere and the Greenland and Antarctic ice sheets. In this set-up, sea-level evolution and climate-ice sheet interactions are modelled in a consistent framework.

Surface mass balance change governed by changes in surface meltwater runoff is the dominant forcing for the Greenland ice sheet, which shows a peak sea-level contribution of 1.4 m at 123 kyr BP in the reference experiment. Our results indicate that ice sheet-climate feedbacks play an important role to amplify climate and sea-level changes in the Northern Hemisphere. The sensitivity of the Greenland ice sheet to surface temperature changes considerably increases when interactive albedo changes are considered. Southern Hemisphere

29   polar and sub-polar ocean warming is limited throughout the Last Interglacial and surface and

30   sub-shelf melting exerts only a minor control on the Antarctic sea-level contribution with a

31   peak of 4.4 m at 125 kyr BP. Retreat of the Antarctic ice sheet at the onset of the LIG is

32   mainly forced by rising sea-level and to a lesser extent by reduced ice shelf viscosity as the

33   surface temperature increases. Global sea level shows a peak of 5.3 m at 124.5 kyr BP, which

34   includes a minor contribution of 0.35 m from oceanic thermal expansion. Neither the

35   individual contributions nor the total modelled sea-level stand show fast multi-millennial time

36   scale variations as indicated by some reconstructions.

37

38   2   Introduction

39   The climate and sea-level evolution of past warm periods in the history of the Earth can give

40   important insights into expected changes in the future. The Last Interglacial (LIG) in

41   particular is often considered as a prime candidate for a potential, albeit limited, analogue for

42   a warmer future world, due to a wealth of available reconstructions of climate and sea level

43   for this period ~130-115 thousand years (kyr) ago (e.g. Dutton et al., 2015). Problems for the

44   direct comparison between LIG and future climates arise mainly from the different forcing

45   responsible for the warming, which can be ascribed to orbital variations during the LIG and to

46   elevated levels of greenhouse gases in the future. During the LIG, global mean annual surface

47   temperature is thought to have been 1°C to 2°C higher and peak global annual sea surface

48   temperatures 0.7°C ± 0.6°C higher than pre-industrial (e.g. Turney and Jones, 2010; McKay

49   et al., 2011), with the caveat that warmest phases were assumed globally synchronous in these

50   data syntheses (Masson-Delmotte et al., 2013). These numbers are largely confirmed by a

51   recent compilation, which resolves the temporal temperature evolution (Capron et al., 2014).

52   Due to polar amplification, high latitude surface temperatures, when averaged over several

53   thousand years, were at least 2°C higher than present (Masson-Delmotte et al., 2013) and

54   were up to 5°C higher over the ice sheets (EPICA community members, 2004; Masson-

55   Delmotte et al., 2015). These high temperatures had severe consequences for the evolution of

56   the ice sheets at the onset and during the LIG as evidenced in large variations of sea level

57   (Rohling et al., 2014; Grant et al., 2012). Coming out of the penultimate glaciation with a sea-

58   level depression of up to 130 m, the global sea level has peaked during the LIG, estimated at

59   5.5 to 9 m higher than today (Dutton and Lambeck, 2012; Kopp et al., 2009; 2013), with a

60   current best estimate of 6 m above the present level (Masson-Delmotte et al., 2013).

A higher-than-present sea-level stand almost certainly implies a complete melting of the Laurentide and Fennoscandian ice sheets and a contribution from the Greenland ice sheet (GrIS), from the Antarctic ice sheet (AIS), or from both. However, ice sheet retreat should not be assumed synchronous in the Northern and Southern hemispheres and between individual ice sheets. Fluctuations in global sea-level during the LIG period (Thompson et al., 2011; Kopp et al., 2013) could be a consequence of differences in the timing of retreat and regrowth between the GrIS and AIS.

Because thus far direct evidence for an AIS contribution to the LIG sea-level high-stand is elusive, support for a contribution from the AIS is usually given as a residual of total sea-level stand minus contributions from the GrIS, thermal expansion (THXP) and glaciers and small ice caps. This illustrates that the attribution problem is so far largely underdetermined. It appears that the lower bound of 5.5 m for the LIG sea-level high-stand (Dutton and Lambeck, 2012; Kopp et al., 2013) could be fully explained by maximum values given in the IPCC AR5 (Masson-Delmotte et al., 2013) for the contributions of the GrIS (1.4 - 4.3 m), glaciers and small ice caps (0.42 ± 0.11 m) and THXP (0.4 ± 0.3 m) combined. However, assuming central estimates for all individual components and the total would indicate an Antarctic contribution of ~ 3 m, which would be in line with the contribution estimated for a collapse of the West Antarctic ice sheet (WAIS) alone (Bamber et al., 2009). An Antarctic component is generally assumed to have foremost come from the WAIS, which is thought to be vulnerable due to its marine-based character. It is often speculated to be sensitive to ocean warming and increased sub-shelf melting (e.g. Duplessy et al., 2007; Holden et al., 2010), possibly caused by the interhemispheric see-saw effect (Stocker, 1998). However, a combination of partial WAIS collapse and some East Antarctic ice sheet (EAIS) retreat is also a possibility due to the large size of the latter. High-end estimates of sea-level change can only be reconciled with an additional EAIS contribution, supposedly from marine-based sectors in the Wilkes and Aurora basins (Pollard et al., 2015; DeConto and Pollard, 2016). One issue complicating the residual argument is the aforementioned possibility of different timing of the GrIS and AIS contributions. Indirect evidence of a WAIS reduction or collapse may come from climate modelling studies that attempt to explain stable-isotope ratios from ice (core) records (Holden et al., 2010; Steig et al., 2015).

The GrIS evolution is somewhat better constrained than the AIS evolution by ice core records both in the central part (GRIP, NGRIP, NEEM) and at the periphery (Dye-3, Camp Century),

93   even if interpretation of the lower parts of the records remains ambiguous. To this date, none
94   of the Greenland ice cores shows continuous and undisturbed information back in time
95   through the LIG and into the penultimate glacial maximum. The relatively high temperatures
96   during the LIG as reconstructed from the folded lower parts of the NEEM ice core (NEEM
97   community members, 2013; Landais et al., 2016) seem to be incompatible with the general
98   view that the ice sheet has lost rather little volume during the LIG (e.g. Robinson et al., 2011;
99   Colville et al., 2011). Several studies have therefore attempted to identify possible biases in
100 the NEEM reconstructions (e.g. van de Berg et al., 2013; Merz et al., 2014; Sjolte et al., 2014;
101 Steen-Larsen et al., 2014; Masson-Delmotte et al., 2015; Merz et al., 2016; Pedersen et al.,
102 2016). Furthermore, the minimum extent and margin position of the northeastern part of the
103 ice sheet is not well constrained, leaving room for alternative retreat scenarios (e.g. Born and
104 Nisancioglu, 2012).

105 Modelling studies of the GrIS for the entire LIG period so far often use parameterised
106 representations of the climate forcing (e.g. Huybrechts, 2002), forcing based on time slice
107 climate experiments (e.g. Born and Nisancioglu, 2012; Stone et al., 2013; Langebroek and
108 Nisancioglu, 2016) or asynchronous coupling (Helsen et al., 2013), while full coupling
109 between ice and climate models is still a challenge and limited to models of intermediate
110 complexity (e.g. Robinson et al., 2011). Ice sheet modelling studies with specific focus on the
111 AIS during the LIG are rare due to the aforementioned lack of climate and geomorphological
112 constraints for that period. However, some results on the AIS during the LIG have been
113 presented in studies with main focus on other time periods (e.g. Huybrechts, 2002) or with
114 interest on longer time scales (e.g. Pollard and DeConto, 2009; de Boer et al., 2013, 2014). A
115 recent study by DeConto and Pollard (2016) utilizes simulations of the AIS during the LIG to
116 constrain future sea-level projections.

117 Despite recent advances (e.g. Capron et al., 2014), the fundamental shortcoming at present for
118 improving modelled constraints on the LIG ice sheet contribution to sea level with physical
119 models is the sparse information on LIG polar climate and oceanic conditions. Consequently,
120 our effort is directed towards studying key mechanisms and feedback processes in the coupled
121 climate-ice sheet system during the LIG. Here, we present modelling results from the first
122 fully coupled climate-ice sheet simulation of the LIG period (135 kyr BP to 115 kyr BP) using
123 ice sheet models of the GrIS and AIS and a climate model of intermediate complexity. In this
124 set-up LIG sea-level evolution and climate-ice sheet interactions can be modelled in a

consistent framework. With focus on climate and ice sheet changes in Greenland and Antarctica and corresponding sea-level changes, we compare results from the fully coupled model to former climate simulations with prescribed ice sheet changes and uncoupled ice sheet experiments. In the following, we describe the model (section 3) and the experimental setup (section 4) and present results (section 5) and conclusions (section 6).

3 Model description

We use the Earth system model of intermediate complexity LOVECLIM version 1.3, which includes components representing the atmosphere, the ocean and sea ice, the terrestrial biosphere and the Greenland and Antarctic ice sheets (Fig. 1). The model has been utilised in a large number of coupled climate-ice sheet studies (e.g. Driesschaert et al., 2007; Swingedouw et al., 2008; Goelzer et al., 2011; 2012). Version 1.2 is described in detail in Goosse et al. (2010). The present set-up of the climate model component is identical to the model used in Loutre et al. (2014) and Goelzer et al. (2016). Where in the latter study the ice sheet components were prescribed and used as forcing for the climate model, in the present work, they are fully two-way coupled with information exchanged every full year. The model components for the GrIS and AIS are three-dimensional thermomechanical ice-dynamic models (Huybrechts and de Wolde, 1999), which have been utilised for long-term stand-alone ice sheet simulations in the past (Huybrechts, 2002). Their behaviour in the coupled system and detailed analysis of the ice sheet mass balance components are described in Huybrechts et al. (2011). The surface mass balance model is based on the positive degree-day (PDD) method (Janssens and Huybrechts, 2000) and distinguishes between snow accumulation, rainfall and meltwater runoff, all parameterized as a function of temperature. Surface melt is estimated based on two distinct PDD factors for ice and snow and may be retained and refreeze in the snow pack. Melt model parameters are unmodified compared to earlier studies (Goosse et al., 2010; Huybrechts et al., 2011) and have been extensively validated for the present day (e.g. Vernon et al., 2013).

Because of the relatively coarse resolution of the atmosphere in LOVECLIM (T21), the higher resolution ice sheet models (10x10 km for Greenland and 20x20 km for Antarctica) are forced with temperature anomalies and precipitation ratios relative to the pre-industrial reference climate. Climate anomalies are interpolated to the ice sheet grids using Lagrange

156 polynomials and the SMB-elevation feedback is accounted for natively in the PDD model on
157 the ice sheet grid.

158 The ice sheet models in turn provide the climate model with changing topography, ice sheet
159 extent (albedo) and spatially and temporally variable freshwater fluxes. The coupling
160 procedure for these variables is unmodified to earlier versions of the model (Goosse et al.,
161 2010), while recent model improvements for the ice-climate coupling interface are described
162 in Appendix A.

3.1 Pre-industrial reference model state

164 A pre-industrial climate state required as a reference for the anomaly forcing mode is
165 generated by running the climate model with fixed present-day modelled ice sheet
166 configuration to a steady state. Standard settings for orbital parameters and greenhouse gas
167 forcing for this experiment are applied following the PMIP3 protocol
168 (https://pmip3.lsce.ipsl.fr/). The present-day ice sheet configurations for the GrIS and AIS are
169 the result of prolonging the same stand-alone ice sheet experiments used to initialise the LIG
170 ice sheet configuration described below towards the present day (Huybrechts and de Wolde,
171 1999; Huybrechts, 2002; Goelzer et al., 2016).

3.2 Northern Hemisphere ice sheet forcing

173 At the onset of the LIG, large Northern Hemisphere (NH) ice sheets other than on Greenland
174 were still present and melted away over the course of several millennia. To account for these
175 ice sheet changes and their impact on climate and ocean evolution, a reconstruction of the
176 penultimate deglaciation of the NH is necessary for our experiments starting in 135 kyr BP.
177 Because there is very little geomorphological evidence for NH ice sheet constraints during
178 Termination II, a reconstruction of NH ice sheet evolution is made by remapping the retreat
179 after the Last Glacial Maximum according to the global ice volume reconstruction (Lisiecki
180 and Raymo, 2005) during the onset of the LIG. The same procedure was already used in
181 earlier work to produce NH ice sheet boundary conditions for climate model simulations
182 (Loutre et al., 2014; Goelzer et al., 2016).

3.3 Modelled sea-level change

The modelled sea-level evolution takes into account contributions from the prescribed NH ice sheets, the GrIS and AIS and the steric contribution due to density changes of the ocean water. The only component not explicitly modelled is the contribution of glaciers and small ice caps, which have been estimated to give a maximum contribution of 0.42 ± 0.11 m during the LIG (Masson-Delmotte et al., 2013) and may contain as much as 5-6 m sea-level equivalent during glacial times (CLIMAP, 1981; Clark et al., 2001).

Changes in the sea-level contribution of the GrIS can be directly related to its net mass balance (MB), composed of snow accumulation (ACC), surface meltwater runoff (RUN), basal melting (BAS) and iceberg calving flux (CAL):

$$MB = ACC - RUN - BAS - CAL$$

Since the GrIS model ignores the small bodies of floating ice in the north, these values are taken over the ice sheet proper only.

For the AIS, CAL is replaced by the flux across the grounding line (GRF) in the definition of the net mass balance of the grounded ice sheet MB_{gr}, which needs further corrections to estimate changes in sea level (see below):

$$MB_{gr} = ACC - RUN - BAS - GRF$$

The net mass balance of Antarctic floating ice shelves MB_{fl} given here for completeness includes GRF as an additional source term, but does not contribute to sea-level changes in our model:

$$MB_{fl} = GRF + ACC - RUN - BAS - CAL$$

The Antarctic contribution to global sea-level change is calculated taking into account corrections for grounded ice replacing seawater, grounded ice being replaced by seawater *and* seawater being replaced by isostatic bedrock movement. These effects are mainly of importance for the marine sectors of the WAIS. Note that these effects are not considered in the climate model, which operates with a fixed present-day land-sea mask. The additional correction for bedrock changes is responsible for a ~3 m lower sea-level contribution at 135 kyr BP compared to taking only changes in volume above floatation into account. This additional sea-level depression arises from depressed bedrock under the load of the ice in the marine sectors of the ice sheet.

213 For the GrIS, the same corrections are applied, where the marine extent of ice grounded
214 below sea level is parameterised. However, the corrections imply only a ~30 cm lower
215 contrast to present-day sea level due to GrIS expansion at 135 kyr BP and ~15 cm higher at
216 130 kyr BP compared to calculations based on the entire grounded ice volume. The change in
217 sign arises from bedrock changes in delayed response to ice loading changes coming out of
218 the penultimate glacial period.

219 The steric component of global sea level considers density changes due to local changes of
220 temperature and salinity, but global salinity is restored as often done in ocean models to
221 guarantee stability.

222

223 **4   Experimental setup**

224 **4.1   Model forcing**

225 All simulations are forced by time-dependent changes in greenhouse gas (GHG)
226 concentrations and insolation running from 135 kyr BP until 115 kyr BP (Fig. 2). The
227 radiative forcing associated with the reconstructed GHG levels is below pre-industrial values
228 for most of this period and hardly exceeds it at ~128 kyr BP (Fig. 2b). The changes in the
229 distribution of insolation received by the Earth are computed from the changes in the orbital
230 configuration (Berger, 1978) and represent the governing forcing during peak LIG conditions
231 (Fig. 2a).

232 In order to account for coastline changes and induced grounding line changes, both ice sheet
233 models are forced by changes in global sea-level stand (Fig. 2c) using a recent sea-level
234 reconstruction based on Red Sea data (Grant et al., 2012). The chronology of this data is
235 thought to be superior compared to sea-level proxies based on scaled benthic $\delta^{18}O$ records
236 (Grant et al., 2012; Shakun et al., 2015). In this sea-level forcing approach, local changes due
237 to geoidal eustasy are not taken into account, which would result in lower amplitude sea-level
238 changes close to the ice sheets, but that would not be consistent with the stand-alone spin-up
239 of the ice sheet models.

240 As mentioned earlier, the ice sheet models are forced with temperature anomalies relative to
241 the pre-industrial reference climate. To ensure a realistic simulation of the GrIS evolution, the
242 temperature anomaly forcing from the climate model over the GrIS needs to be rescaled. In

243 absence of such scaling, the ice sheet almost completely melts away over the course of the
244 LIG in disagreement with the ice core data, which suggests a large remaining ice sheet during
245 the LIG (Dansgaard et al., 1982; NEEM community members, 2013). In the absence of firm
246 constraints on the climate evolution over the ice sheet, the temperature scaling in the present
247 study represents a pragmatic solution to produce a GrIS evolution reasonably in line with ice
248 core constraints on minimum ice sheet extent during the LIG. The scaling is only applied for
249 the GrIS, since we have not identified a physical process that would justify a similar
250 procedure for to the AIS.

4.2   Reference simulation and sensitivity experiments

252 Our reference simulation is a fully coupled experiment with a uniform scaling of the
253 atmospheric temperature anomaly over Greenland with a factor of R=0.4, which was chosen
254 to give a good match to constraints on minimum extent of the GrIS during the LIG.
255 Additional sensitivity experiments are listed in Table 1 and are described in the following.

256 Two sensitivity experiments with modified scaling (R=0.5, 0.3) are added to evaluate the
257 impact on the results. The range of parameter R is chosen to retain an acceptable agreement of
258 the minimum GrIS extent during the LIG with reconstructions. In practice, the high scaling
259 factor (R=0.5) is chosen to produce the smallest minimum ice sheet extent, which still has ice
260 at the NEEM site. The low scaling factor (R=0.3) was adopted to produce the smallest
261 minimum ice sheet extent, which is still covering Camp Century.

262 The three fully coupled experiments are complemented by additional sensitivity experiments,
263 in which the ice sheet models are forced with (modified) climate forcing produced by the
264 fully coupled reference run. These experiments serve to study ice sheet sensitivity in response
265 to changes in the climate forcing and are also used to evaluate ice sheet-climate feedbacks by
266 comparing the coupled and uncoupled system. The ice sheet evolution in the forced reference
267 experiment (ice sheet model run offline with the recorded climate forcing of the coupled
268 reference run) should by construction be identical to the response in the fully coupled run, and
269 only serves as a control experiment. Two additional forced experiments have been run with
270 modified temperature scaling for the GrIS (R=0.5, 0.3), which can be directly compared to the
271 respective fully coupled experiment.

272　For the AIS, an experiment with suppressed sub-shelf melting has been performed to isolate

273　the effect of ocean temperature changes on the ice volume evolution and sea-level

274　contribution.

275　**4.3　Initialisation of the reference simulation**

276　The goal of our initialisation technique is to prepare a coupled ice sheet-climate model state

277　for the transient simulations starting at 135 kyr BP exhibiting a minimal coupling drift. Both

278　ice sheet models are first integrated over the preceding glacial cycles in order to carry the

279　long-term thermal and geometric history with them (Huybrechts and de Wolde, 1999;

280　Huybrechts, 2002; Goelzer et al., 2016). The climate model is then initialized to a steady state

281　with ice sheet boundary conditions, greenhouse gas forcing and orbital parameters for the

282　time of coupling (135 kyr BP). When LOVECLIM is integrated forward in time in fully

283　coupled mode, the climate component is already relaxed to the ice sheet boundary conditions.

284　The mismatch between stand-alone ice sheet forcing and climate model forcing is

285　incrementally adjusted in the period 135-130 kyr BP with a linear blend between the two to

286　minimize the effect of changing boundary conditions for the ice sheet model. A small,

287　unavoidable coupling drift of the ice sheet component arises from a switch of spatially

288　constant to spatially variable temperature and precipitation anomalies at the time of coupling,

289　but is uncritical to the results.

290

291　**5　Results**

292　The modelled LIG climate evolution and comparison with proxy reconstructions were

293　presented in detail in two earlier publications (Loutre et al., 2014; Goelzer et al., 2016) for the

294　same climate model setup. In the following, we focus on differences to those two works that

295　arise from a different ice sheet evolution and from the incorporation of feedbacks between

296　climate and ice sheets that are taken into account in our present, fully coupled approach. In

297　addition, we present results pertaining to the ice sheet evolution and simulated sea-level

298　changes.

299　**5.1　Climate evolution**

300　Global annual mean near-surface air temperature in the reference experiment (Fig. 3) shows a

301　distinct increase until 129 kyr BP in response to orbital and greenhouse gas forcing (Fig. 2)

and to an even larger extent in response to changes in ice sheet boundary conditions. The peak warming reaches 0.3 °C above the pre-industrial at 125.5 kyr BP. Thereafter, cooling sets in and continues at a much lower rate compared to the rate of warming before 129 kyr BP. The importance of ice sheet changes is illustrated by comparing the reference experiment with a climate simulation (Loutre et al., 2014) forced by insolation and GHG changes only (noIS) and with a one-way coupled climate model run (Goelzer et al., 2016) forced with prescribed NH, Antarctic and Greenland ice sheet changes (One-way). The fully coupled experiment exhibits a global mean temperature evolution during the LIG, which is very similar to One-way (Fig. 3). A much larger temperature contrast at the onset of the LIG in the reference experiment compared to noIS arises mainly from changes in surface albedo and melt water fluxes of the NH ice sheets, which freshen the North Atlantic and lead to a strong reduction of the Atlantic meridional overturning circulation (Loutre et al., 2014). All three simulations show only small differences in the global mean temperature evolution after 127 kyr BP. The episode of relative cooling in the reference experiment with a local temperature minimum at 128 kyr BP is due to cooling of the Southern Ocean (SO) and sea-ice expansion in response to large Antarctic freshwater fluxes caused mainly by the retreat of the WAIS. This mechanism was already described by Goelzer et al. (2016), but now occurs 2 kyr later in the fully coupled experiment, due to a modified timing of the AIS retreat. The effect of including ice-climate feedbacks by means of a two-way coupling is otherwise largely limited to the close proximity of the ice sheets as discussed in the following.

5.2 Greenland ice sheet

The Greenland ice sheet evolution over the LIG period is largely controlled by changes in the surface mass balance dominated by surface meltwater runoff (Fig. 4c). Specifically, summer surface melt water runoff from the margins is the dominant mass loss of the GrIS after 130 kyr BP, when the ice sheet has retreated largely on land. Due to increased air temperatures over Greenland, the mean accumulation rate (averaged over the ice covered area) is consistently above the present-day reference level after 128 kyr BP, but increases to at most 18% higher (not shown). In contrast, net accumulation over grounded ice (Fig. 4b) is strongly modulated by the retreat of the ice sheet and exhibits a marked increase towards the end of the simulation as ice sheet grows again and into regions with higher precipitation. Conversely, surface meltwater runoff over the Greenland ice sheet shows an up to threefold increase compared to the present day at the beginning with consistently higher-than present values

334   between 130.5 kyr to 120.5 kyr BP (Fig. 4c). Temperature anomalies responsible for the

335   increased runoff are on average above zero between 129.5 kyr to 120.5 kyr BP and peak at 1.3

336   °C (after scaling) around 125 kyr BP (Fig. 4a). The calving flux (Fig. 4d) decreases as surface

337   melting and runoff (Fig. 4c) increase, removing some of the ice before it can reach the coast

338   and also as the ice sheet retreats from the coast (cf. Fig. 5), in line with decreasing area and

339   volume (Fig. 4f). In the second half of the experiment, runoff decreases with decreasing

340   temperature anomalies and the calving flux increases again with increasing ice area and

341   volume. The net mass balance of the ice sheet (Fig. 4e) reflects the compounded effect of all

342   components with negative values before and positive values after the time of minimum

343   volume.

344   Entering the warm period, the furthest retreat of the ice sheet occurs in the southwest and

345   northwest (Fig. 5), accompanied by an overall retreat from the coast. At the same time, the ice

346   sheet gains in surface elevation over the central dome due to increased accumulation. By 115

347   kyr BP, the ice sheet has regrown beyond its present-day area almost everywhere and contact

348   with the ocean is increasing. The GrIS volume change implies a sea-level contribution peak of

349   1.4 m at 123 kyr BP (Fig. 11a). For the two sensitivity experiments (High, Low) with

350   modified scaling (R=0.5, 0.3), the contribution changes to 2.7 m and 0.65 m, respectively,

351   crucially controlled by the scaling factor (Table 2).

352   NEEM ice core data (NEEM community members, 2013) and radiostratigraphy of the entire

353   ice sheet (MacGregor et al., 2015) indicate that the NEEM ice core site was ice covered

354   through the entire Eemian as is the case for our reference experiment. Elevation changes from

355   that ice core are however not very well constrained and even if they were, would leave room

356   for a wide range of possible retreat patterns of the northern GrIS (e.g. Born and Nisancioglu,

357   2012). The Camp Century ice core record contains some ice in the lowest part with a colder

358   signature then ice dated as belonging to the Eemian period (Dansgaard et al., 1982). It is

359   likely that this ice is from before the Eemian even in view of possible disturbance of the lower

360   levels, which was shown to exist for the NEEM core site (NEEM community members,

361   2013). In view of this evidence, the northwestern retreat of the ice sheet in our reference

362   simulation may be too far inland, as a direct result of the largely unconstrained climatic

363   forcing in this area. It was shown that a different climate forcing could produce a larger

364   northern retreat still in line with the (limited) paleo evidence (Born and Nisancioglu, 2012).

365   Some more thinning and retreat in the south is also possible without violating constraints on

366   minimal ice sheet extent from Dye-3 (Dansgaard et al., 1982). LIG ice cover of the Dye-3 site

367   is not a necessity when taking into consideration that older ice found at the base of the core

368   could have flowed in from a higher elevation.

369   A comparison of modelled temperatures in North-East Greenland (Fig. 6) shows differences

370   of up to 5 degrees between annual mean and summer temperatures in the reference

371   experiment. Comparison with temperature reconstructions based on the NEEM ice core

372   record indicates that the steep temperature increase marking the onset of the LIG occurs 2-3

373   kyr earlier in the model compared to the reconstructions. The amplitude of modelled summer

374   temperatures attains levels of the central estimate, while annual mean temperatures fall in the

375   lower uncertainty range of the reconstructions. Temperatures exceeding the central estimate

376   are only reached in the One-way experiment, which exhibits a somewhat different retreat

377   pattern of the GrIS due to the different climate forcing (Goelzer et al., 2016).

378   The strength of the ice-climate feedback on Greenland was examined by comparing additional

379   experiments in which the coupling between ice sheet and climate is modified. Results from

380   the fully coupled model are compared to those from forced ice sheet runs that are driven with

381   the climate forcing from the coupled reference model run (Table 2 and Fig. 7a). The scaling

382   of Greenland forcing temperature is set to a magnitude of 0.3 (Forced low), 0.4 (Forced

383   reference) and 0.5 (Forced high), respectively. When the feedback between ice sheet changes

384   and climate is included in the coupled experiments, the warming over the margins is

385   considerably increased (reduced) for experiment High (Low) compared to the respective

386   forced experiments. Consequently, ice volume changes show a non-linear dependence on the

387   temperature scaling for the fully coupled run, while they are near linear for the forced runs

388   (Table 2 and Fig. 7a). The dominant (positive) feedback mechanism arises from how

389   changing albedo characteristics are taken into account for a melting ice sheet surface (Fig.

390   7b). The underlying surface type with different characteristic albedo values for tundra and ice

391   sheet is determined by the relative amount of ice cover, which is modified when the area of

392   the ice sheet is changing. On much shorter time scales, the albedo can change due to changes

393   in snow depth and also due to changes of the snow cover fraction, which indicates how much

394   surface area of a grid cell is covered with snow (Fig. 7b). Both snow processes lead to lower

395   albedo and increased temperatures in places where the ice sheet starts melting at the surface.

396   The difference in warming between forced and fully coupled experiments is however located

397   over the ice sheet margins and this does not have a considerable influence on the NH or

global temperature response. The snow albedo effects are near-instantaneous and their importance for the ice sheet response underline earlier findings that a basic albedo treatment is an essential aspect of a coupled ice–climate modelling system (e.g. Robinson and Goelzer, 2014). A comparatively smaller effect and operating on much longer time scales arises from the retreating ice sheet margin being replaced by tundra with a lower albedo (Fig. 7b).

5.3 Antarctic ice sheet

The annual mean air temperature anomaly over Antarctica (averaged over grounded ice) increases at the beginning of the experiment to reach a peak of up to 2°C at 125 kyr BP (Fig. 8a), before cooling sets in and continues until 115 kyr BP. The warming before the peak is around a factor two faster than the cooling afterwards, with both transitions being near linear on the millennial time scale. The surface climate over the AIS appears to be largely isolated from millennial time scale perturbations occurring in the SO in response to changing freshwater fluxes in both hemispheres (Goelzer et al., 2016). While freshwater fluxes from the retreating AIS itself lead to sea-ice expansion and surface cooling in the SO, freshwater fluxes from the decay of the NH ice sheets are communicated to the Southern Hemisphere (SH) by the interhemispheric see-saw effect (Goelzer et al., 2016). Pre-industrial surface temperature levels are first reached at 128 kyr BP and then again at 118 kyr BP after cooling throughout the second half of the experiment. The accumulation (over grounded ice) shows an initial increase in line with the higher temperatures until 130 kyr BP (Fig. 8b) but records a changing grounded ice sheet area further on, which mostly follows the marked retreat and later slow regrowth of the ice sheet. Relative to the pre-industrial, the mean accumulation rate (averaged over grounded ice) increases at most 20 % in annual values and up to 12 % for the long-term mean (not shown). As a consequence of the surface forcing, the AIS shows a small volume gain until 130.5 kyr BP (Fig. 8f) due to increase in precipitation before a large-scale retreat of the grounding line sets in. The surface meltwater runoff over grounded ice equally increases with increasing temperature (Fig. 8c) but remains of negligible importance (note difference of vertical scales between panel b and c in Fig. 8) for the net mass balance (Fig. 8e) of the ice sheet. This is also the case for basal melting under the grounded ice sheet (not shown).

Changes in the sub-shelf melt rate play an important role for the present mass balance of the AIS and are often discussed as a potential forcing for a WAIS retreat during the LIG (e.g. Duplessy et al., 2007; Holden et al., 2010) and during the last deglaciation (Golledge et al.,

14

429   2014). The average sub-shelf melt rate diagnosed for the area of the present-day observed ice

430   shelves in our reference simulation (Fig. 8d) increases to at most 20 % above the pre-

431   industrial with a peak in line with the air temperature maximum (Fig. 8a, d). However, ocean

432   warming to above pre-industrial temperatures occurs already before 130 kyr BP (not shown),

433   more than 2 kyr earlier compared to the air temperature signal. This is a consequence of the

434   interhemispheric see-saw effect (Stocker, 1998), which explains SO warming and cooling in

435   the North Atlantic as a consequence of reduced oceanic northward heat transport due to a

436   weakening of the Atlantic meridional overturning circulation (Goelzer et al., 2016).

437   Ice sheet area and volume (Fig. 8f) decrease rapidly between 129 and 127 kyr BP, and

438   indicate a gradual regrowth after 125 kyr BP, also visible in the net mass balance (Fig. 8e).

439   Those changes arise mainly from a retreat and re-advance of the WAIS (Fig. 9). In our model,

440   the ice sheet retreat exhibits characteristics of an overshoot behaviour due to the interplay

441   between ice sheet retreat and bedrock adjustment. The rebound of the bedrock, which is

442   initially depressed under the glacial ice load, is delayed compared to the relatively rapid ice

443   sheet retreat, giving rise to a grounding-line retreat well beyond the pre-industrial steady-state

444   situation. These results are in line with earlier work with a stand-alone ice sheet model

445   (Huybrechts, 2002), but also rely on a relatively large glacial-interglacial loading contrast in

446   these particular models. The sea-level contribution above the present-day level from the AIS

447   peaks at 125 kyr BP at 4.4 m (Fig. 11b).

448   Sensitivity experiments, in which specific forcing processes are suppressed, show that surface

449   melting (not shown) and sub-shelf melting play a limited role for the AIS retreat in our

450   experiments. The sea-level contribution peak in an experiment with suppressed sub-shelf

451   melting (Fig. 11b) is about 40 cm lower compared to the reference experiment and remains

452   around one meter lower between 123 kyr BP until the end of the experiment. The difference

453   between the experiments at a given point in time arises from a lower overall sea-level

454   contribution when sub-shelf melting is suppressed, but also from a difference in timing

455   between both cases. The dominant forcing for the AIS retreat in our model is a combination

456   of rising global sea level and increasing surface temperature, which leads to increasing

457   buoyancy and reduced ice shelf viscosity, respectively. The relative timing between sea-level

458   forcing (Fig. 2c) and temperature forcing (Fig. 8a) is therefore of critical importance for the

459   evolution of the ice sheet at the onset of the LIG.

15

460   The limited effect of surface melting and sub-shelf melting on the sea-level contribution is
461   ultimately due to a limited magnitude of surface temperature and ocean temperature changes.
462   The limited Antarctic and SO temperature response has already been highlighted in earlier
463   studies with the same climate component (Loutre et al., 2014; Goelzer et al., 2016) and is
464   confirmed here with a fully coupled model. The feedback mechanism suggested by Golledge
465   et al. (2014) for Termination I, which draws additional heat for sub-shelf melting from
466   freshwater-induced SO stratification and sea-ice expansion is also active in our experiment,
467   but too short-lived and of too little amplitude to lead to substantially increased melt rates. Our
468   limited AIS response to climatic forcing is also in line with other modelling results for the
469   LIG period (Pollard et al., 2015), albeit with a different forcing strategy, where substantial
470   retreat of marine based sectors of the EAIS can only be achieved by including special
471   treatment of calving fronts and shelf melting, which was not included here.

472   As mentioned earlier, direct constraints of the AIS configuration during the LIG are still
473   lacking. Goelzer et al. (2016) suggested that the timing of the main glacial-interglacial retreat
474   of the AIS could be constrained by a freshwater induced oceanic cold event recorded in ocean
475   sediment cores (Bianchi and Gersonde et al., 2002). The main retreat in their one-way
476   coupled climate model run happened ~129.5 kyr BP, a timing predating the time of retreat in
477   the fully coupled model by ~2 kyr due to the difference in atmospheric and oceanic forcing.
478   This lag is also visible in modelled temperature changes over the East Antarctic ice sheet
479   (EAIS) that have been compared to temperature reconstructions for four ice core locations
480   (Fig. 10). One-way and Reference show a larger temperature contrast, better in line with the
481   ice core data, compared to the experiment with a fixed ice sheet (noIS). However, the timing
482   of warming was better matched in One-way with an earlier ice sheet retreat.

483   It is noteworthy in this context that the prescribed sea-level forcing imposes an important
484   control on the timing of the Antarctic retreat and is a source of large uncertainty. We have
485   only used the central estimate of the Grant et al. (2012) sea-level reconstruction, but
486   propagated dating uncertainties could accommodate a shift of the forcing by up to 1 kyr either
487   way. Former experiments (not shown) have indicated that the main retreat appears another 2
488   kyr later when a sea-level forcing based on a benthic $\delta^{18}O$ record (Lisiecki and Raymo, 2005)
489   is used instead of the sea-level reconstruction of Grant et al. (2012).

490

5.4 Thermal expansion of the ocean

The steric sea-level component due to ocean thermal expansion (Fig. 11c) is largely following the global temperature evolution (Fig. 3), but is also strongly modified by changes in ice sheet freshwater input. Ocean expansion is rapid during peak input of freshwater and stagnant during episodes of decreasing freshwater input. This is because the net ocean heat uptake is large when freshwater input peaks, which happens in three main episodes in our experiment. Two episodes of freshwater input from the NH centred at 133.6 and 131.4 kyr BP are followed by an episode of combined input from the NH and the AIS centred at 128.2 kyr BP (not shown). The anomalous freshwater input leads to stratification of the surface ocean, sea-ice expansion and reduction of the air-sea heat exchange, effectively limiting the ocean heat loss to the atmosphere. This implies that global sea-level rise due to ice sheet melting is (weakly and temporarily) amplified by the freshwater impact on ocean thermal expansion. We simulate a peak sea-level contribution from thermal expansion of 0.35 m at 125.4 kyr BP, which forms part of a plateau of high contribution between 127.3 and 124.9 kyr BP (Fig. 11c). The amplitude is within the range of current estimates of 0.4 ± 0.3 m (McKay et al., 2011; Masson-Delmotte et al., 2013).

5.5 Global sea-level change

Combining contributions from GrIS, AIS and thermal expansion, global sea level peaks at ~5.3 m at 124.5 kyr BP (Fig. 12c) with a slow decrease thereafter as first the AIS and 2 kyr later the GrIS start to regrow. For the AIS the model indicates a clear asymmetry between relatively fast retreat and much slower regrowth (Fig. 12b).

Modelled GrIS and AIS sea-level contributions together with prescribed NH sea level are within the 67% confidence interval of probabilistic sea-level reconstructions (Kopp et al., 2009) for the period ~125-115 kyr BP (Fig. 12). The last 20 m rise in sea-level contributions from the NH (including Greenland) is steeper and occurs 1~2 kyr earlier in our model compared to what the reconstructions suggest, which is consequently also the case for the rise in global sea level at the onset of the LIG. The Antarctic retreat in our model is more rapid compared to the reconstruction and does not show the regrowth ~131-129 kyr BP suggested by the data from Kopp et al. (2009). The modelled ice sheet evolution in our reference run reproduces well the global average sea-level contribution 125-115 kyr BP based on the best

522   estimate of Kopp et al. (2009) when taking into account the modelled steric contribution (0.35

523   m) and assuming a maximum possible contribution (0.42+-0.11 m) of glaciers and small ice

524   caps (Masson-Delmotte et al., 2013). The multi-peak structure of global sea-level

525   contributions during the LIG suggested by the median reconstructions (Kopp et al., 2009;

526   2013) is not reproduced with our model (Fig. 12c), mainly owing to the lack of such variation

527   in the climate forcing and to the long response times of the ice sheets during regrowth to

528   changing climatic boundary conditions.

529

530   ## 6   Discussion

531   ### 6.1   Global sea-level change

532   While the median projections in Kopp et al., (2009) visually suggest a double-peak structure

533   in the global sea-level evolution during the LIG, our results show that the uncertainty range is

534   wide enough to accommodate a global sea-level trajectory based on physical models without

535   intermediate low stand. The simulated climate forcing in our case does not favour the

536   presence of such variability, which admittedly could be due to missing processes or feedbacks

537   in our modelling. Nevertheless, based on our own modelling results and the Kopp et al.,

538   (2009) reconstruction we are not convinced reproducing a double peak structure is a given

539   necessity.

540   ### 6.2   Greenland ice sheet evolution

541   The temperature anomaly over central Greenland in the coupled model shows a flat maximum

542   around 127 kyr BP (Fig. 4a), similar to the global temperature evolution, but 2 kyr earlier

543   compared to the NEEM reconstruction (NEEM community members, 2013). If assuming

544   present-day configuration and spatially constant warming, ice mass loss from the GrIS could

545   be expected to occur approximately as long as the temperature anomaly remains above zero,

546   which is the case until ~ 122 kyr BP in our reference model and until ~ 119 kyr BP in the

547   NEEM reconstruction. With a lower surface elevation, the time the ice sheet starts to gain

548   mass again would be further delayed. Even with considerable uncertainty due to uncertain

549   spatial pattern of the warming, which modifies this simple reasoning, it is clear that the peak

550   sea-level contribution from the GrIS has to occur late during the LIG. This argument is

551   confirmed by our model results and in line with conclusions recently drawn by Yau et al.

552   (2016) based on data from another Greenland ice core and modelling. Based on the same
553   argument, there is no evidence in the reconstructed NEEM temperature evolution suggesting a
554   regrowth or substantial pause of melting of the GrIS any time during the LIG.

555   The need for scaling the temperature forcing to produce a realistic GrIS evolution would
556   equally apply when our ice sheet model were forced directly with the temperature
557   reconstructed from the NEEM ice core record (NEEM community members, 2013). It appears
558   that practically any ice sheet model with (melt parameters tuned for the present day) would
559   project a near-complete GrIS meltdown, if the amplitude and duration of warming suggested
560   by the NEEM reconstructions would apply for the entire ice sheet. This problem would be
561   further amplified if insolation changes were explicitly taken into account in the melt model
562   (van de Berg et al., 2011; Robinson and Goelzer, 2014). We refer to this mismatch between
563   reconstructed temperatures and assumed minimum ice sheet extent as the "NEEM paradox"
564   (see also Landais et al., 2016). Several attempts to solve this paradox have been made by
565   suggesting possible biases in the interpretation of the relationship between isotope ratio and
566   temperature, which may not be assumed temporally and spatially constant (e.g. Merz et al.,
567   2014; Sjolte et al., 2014; Steen-Larsen et al., 2014; Masson-Delmotte et al., 2015) or may be
568   affected by changes in the precipitation regime (van de Berg et al., 2013) and sea ice
569   conditions (Merz et al., 2016; Pedersen et al., 2016). From a modelling point of view, the
570   decisive question is over what spatial extent and when during the year the temperature
571   reconstruction (and possible future reinterpretations) for the NEEM site should be assumed. A
572   central Greenland warming of large magnitude could only be reconciled with the given
573   geometric constraints if a (much) lower warming was present over the margins and during the
574   summer, which is where and when the majority of the mass loss due to surface melting is
575   taking place.

576   **6.3   Antarctic ice sheet evolution**

577   The main forcing for WAIS retreat during Termination II and the LIG was found to be global
578   sea-level rise from melting of the NH ice sheets, and to a lesser extent surface warming
579   causing a gradual thinning of the ice shelves as the ice softened, contributing to an additional
580   grounding-line retreat as there is less buttressing and increased thinning at the grounding line.
581   These processes also played during Termination I and into the Holocene in simulations with
582   the same ice sheet model (Huybrechts, 2002), but did not produce an overshoot in the sense
583   that the WAIS retreated further inland from its present-day extent. The difference in

584 behaviour between the LIG and the Holocene is mainly the speed of sea-level rise, which was
585 slower during Termination I, and the fact that the global sea-level stand itself did not
586 overshoot the present-day level during the Holocene, giving a less strong forcing. Of
587 particular importance to generate overshoot behaviour is the speed of sea-level rise relative to
588 the speed of bedrock rebound as both control the water depth at the grounding line and hence,
589 grounding-line migration because of the criterion for floatation (hydrostatic equilibrium). If
590 the sea-level rise is fast compared to the bedrock uplift, grounding line retreat will be
591 enhanced, as was the case during Termination II in our model experiments. In that case, the
592 grounding line is able to retreat to a more inland position until the lagged bedrock rebound
593 halts and reverses the process. If on the contrary, the bedrock rebound after ice unloading is
594 fast compared to the sea-level rise, this will tend to dampen grounding-line retreat, as shown
595 in the sensitivity experiments discussed in Huybrechts (2002).

596 Ice shelf viscosity changes also played a role during Termination II and the LIG, but were not
597 found to be the dominant forcing. The response time of viscosity changes in the ice shelves is
598 governed by vertical heat transport, having a typical characteristic time scale of 500 years
599 with respect to surface temperature (Huybrechts and de Wolde, 1999). The mechanism can
600 only be effective over longer time scales and for a limited warming such as occurred during
601 the LIG as otherwise the ice shelves would largely disintegrate from both surface and basal
602 melting. In future warming scenarios, the effect of shelf viscosity changes is therefore usually
603 too slow compared to the anticipated direct effect of increased surface and basal melting rates.
604 For instance, in the future warming scenarios performed with LOVECLIM under $4xCO_2$
605 conditions (Huybrechts et al., 2011), shelf melt rates increased 5-fold, and the ice shelves
606 were largely gone before they had a chance to warm substantially. The implication is that
607 analogies between these different time periods should be reserved on account of different
608 processes playing at different time scales.

6.4 Comparison with other work

610 An earlier attempt to model the coupled climate-ice sheet evolution for the Greenland ice
611 sheet over the LIG period (Helsen et al., 2013) applied an asynchronous coupling strategy to
612 cope with the computational challenge of such long simulations. While it can be assumed that
613 their high-resolution regional climate model provides a more accurate climate forcing
614 compared to our approach, we still lack substantial climate and ice sheet reconstructions for
615 the LIG period to effectively validate model simulations. This applies to the simulated climate

616   as well as to the resulting ice sheet geometries, limiting attempts to constrain the GrIS sea-

617   level contribution to arrive at relatively large and overlapping uncertainty ranges (e.g.

618   Robinson et al., 2011; Stone et al., 2013; Helsen et al., 2013; Langebroek and Nisancioglu,

619   2016). Incidentally, our range of modelled GrIS sea-level contribution is in very close

620   agreement with recent results from a large ensemble study of the LIG sea-level contribution

621   constrained against present-day simulations and elevation changes at the NEEM ice core site

622   (Calov et al., 2015). Despite a possible degree of coincidence in this particular case, the

623   overlap between results reached by largely different methods is indicative of the lack of better

624   constraining data needed to arrive at much narrower uncertainty ranges.

625   **6.5   Model limitations**

626   Simulating the fully coupled ice sheet-climate system for the entire duration of the LIG as

627   presented here is an important step forward for a better understanding of the Earth system

628   during this period. However, our attempt deserves a critical discussion of the limitations of

629   the model setup.

630   A so far unavoidable side effect to running a fully coupled model for several thousands of

631   years is the limited horizontal resolution of the atmospheric model. The katabatic wind effect

632   discussed by Merz et al. (2014) and other small-scale circulation patterns are therefore likely

633   underrepresented. A quantification of how much the strength of ice sheet-climate feedbacks

634   depends on spatial resolution of the climate model would be an interesting study, but is not

635   something we could add to with our model set-up.

636   The applied PDD scheme has been extensively validated with results of more complex

637   Regional Climate Models for simulations of the recent past (e.g. Vernon et al., 2013), but

638   several studies point to limitations of this type of melt model when applied for periods in the

639   past with a different orbital configuration (e.g. van de Berg et. al., 2011; Robinson and

640   Goelzer, 2014). Their results indicate that the stronger northern summer insolation during the

641   LIG should result in additional surface melt on the Greenland ice sheet compared to

642   simulations based on temperature changes alone. We note that this suggests an

643   underestimation of LIG melt with the PDD model and increased melt if it was corrected for.

644   Thus, including an additional melt contribution due to insolation would further increase the

645   contrast of the NEEM paradox in our simulation. Our modelling therefore provides no

646 arguments to support the contention that the limited LIG warming implied over Greenland
647 would be indicative of an overly sensitive ice sheet and mass balance model.

648 Instead, the applied scaling of the temperature anomaly forcing for the GrIS is a necessity to
649 keep the ice sheet from losing too much mass during the warm period and to maintain ice
650 sheet retreat to within limits of reconstructions. Clearly, this implies a limited predictive
651 capability of our model, which is now forced to comply with the given constraints on
652 minimum ice extent during the LIG. However, the Antarctic simulation would not be strongly
653 affected by changes in the melt model due to the limited role of surface melting for the
654 evolution of the AIS during the LIG.

655 The sea-saw effect evoked by NH freshwater forcing leads to millennial time scale
656 temperature variations in the SO, but the surface climate over the AIS is hardly affected in our
657 simulations. Despite some improvement when ice sheet changes are included, the limited
658 Antarctic temperature response appears to be a general feature of the LOVECLIM model (e.g.
659 Menviel et al., 2015), which fails to reproduce a several degree warming during the LIG
660 reconstructed at deep ice core locations. We suspect that the limited resolution of the
661 atmospheric model contributes to this shortcoming but we have not been able to quantify that.

662 ## 6.6 Possible improvements

663 Uncertainty in the age model of the Grant et al. (2012) sea-level reconstruction could in
664 principle be used to force the AIS to an earlier retreat, better in line with the Kopp et al.
665 (2009) reconstructions. We have not attempted that, since other uncertainties, in particular in
666 the climate forcing are large and do not warrant to attempt a precise chronology. Earlier
667 experiments (not shown) indicate however that using a benthic δ^{18}O-stack (Lisiecki and
668 Raymo, 2005) would lead to an even later retreat of the AIS and thus increase the mismatch
669 with the Kopp et al. (2009) reconstruction. Ultimately, it would be desirable to apply a
670 consistent sea-level forcing, based on physical models (e.g. de Boer et al., 2014). However,
671 this would require a prognostic model of NH ice sheet evolution (e.g. Zweck and Huybrechts,
672 2005) and a general solution of the sea-level equation, which would considerably increase
673 complexity and required resources.

674 Targeting model limitations described in the previous sub-section hinges to a large extent on
675 improving the atmospheric component of the climate model, which equally goes hand in hand
676 with an increase in needed computational resources. Given the large remaining uncertainties

677 in the climate forcing during the LIG and a limited impact of an improved physical
678 approximation for ice flow applied to future projections (Fürst et al., 2013), we consider
679 improving the representation of ice sheet dynamics as of secondary importance. However,
680 fully physical treatment of the surface mass balance solution in a coupled climate-ice sheet
681 model framework, as currently targeted by several groups (e.g. Nowicki et al., 2016) appears
682 like a promising development that may eventually be applied for paleo applications such as
683 the transient LIG simulations of interest in the present paper.

684

685 **7   Conclusion**

686 We have presented the first coupled transient simulation of the entire LIG period with
687 interactive Greenland and Antarctic ice sheet components. In our results, both ice sheets
688 contribute to the sea-level high stand during the Last Interglacial, but are subject to different
689 forcing and response mechanisms. While the GrIS is mainly controlled by changes in surface
690 melt water runoff, the AIS is only weakly affected by surface and sub-shelf melting. Instead,
691 grounding line retreat of the AIS is forced by changes in sea level stand and to a lesser extent
692 surface warming, which lowers the ice shelf viscosity. The peak GrIS contribution in our
693 reference experiment is 1.4 m. However, this result is strongly controlled by the need to scale
694 the climate forcing to match existing ice core constraints on minimal ice sheet extent. This
695 shortcoming in our modelling reflects the NEEM paradox, that strong warming over the ice
696 sheet coincides with limited mass loss from the GrIS, indicative of a fundamental missing link
697 in our understanding of the LIG ice sheet and climate evolution. The Antarctic contribution is
698 4.4 m predominantly sourced from WAIS retreat. The modelled steric contribution is 0.35 m,
699 in line with other modelling studies. Taken together, the modelled global sea-level evolution
700 is consistent with reconstructions of the sea-level high stand during the LIG, but no evidence
701 is found for sea-level variations on a millennial to multi-millennial time scale that could
702 explain a multi-peak time evolution. The treatment of albedo changes at the atmosphere-ice
703 sheet interface play an important role for the GrIS and constitute a critical element when
704 accounting for ice sheet-climate feedbacks in our fully coupled approach. Large uncertainties
705 in the projected sea-level changes remain due to a lack of comprehensive knowledge about
706 the climate forcing at the time and a lack of constraints on LIG ice sheet extent, which are
707 limited for Greenland and virtually absent for Antarctica.

708

8   Data availability

The LOVECLIM version 1.3 model code can be downloaded from http://www.elic.ucl.ac.be/modx/elic/index.php?id=289.

Appendix A: Ice-climate coupling improvements

Compared to earlier versions of the model (Goosse et al., 2010), recent model improvements for the coupling interface between climate and ice sheets have been included for the present study. Ocean temperatures surrounding the AIS are now used directly to parameterise spatially explicit sub-ice-shelf melt rates, defining the flux boundary condition at the lower surface of the AIS in contact with the ocean. The sub-shelf basal melt rate M_{shelf} is parameterised as a function of local mid-depth (485-700 m) ocean-water temperature T_{oc} above the freezing point T_f (Beckmann and Goosse, 2003):

$$M_{shelf} = \rho_w c_p \gamma_T F_{melt} (T_{oc} - T_f) / L\rho_i,$$

where ρ_i=910 kg m^{-3} and ρ_w=1028 kg m^{-3} are ice and seawater densities, c_p=3974 J kg^{-1} °C^{-1} is the specific heat capacity of ocean water, γ_T= 10^{-4} is the thermal exchange velocity and L=3.35 x 10^5 J kg^{-1} is the latent heat of fusion. The local freezing point is given (Beckmann and Goosse, 2003) as

$$T_f = 0.0939 - 0.057 \cdot S_0 + 7.64 \times 10^{-4} z_b,$$

with a mean value of ocean salinity S_0=35 psu and the bottom of the ice shelf below sea level z_b. A distinction is made between protected ice shelves (Ross and Ronne-Filchner) with a melt factor of F_{melt} = 1.6x10^{-3}m s^{-1} and all other ice shelves with a melt factor of F_{melt} = 7.4x10^{-3}m s^{-1}. The parameters are chosen to reproduce observed average melt rates (Depoorter et al., 2013) under the Ross, Ronne-Filchner and Amery ice shelves for the pre-industrial LOVECLIM ocean temperature and Bedmap2 (Fretwell et al., 2013) shelf geometry. For ice shelves located inland from the fixed land-sea mask of the ocean model, mid-depth ocean temperature from the nearest deep-ocean grid point in the same embayment is used for the parameterisation.

24

In addition, surface melting of the Antarctic ice shelves has been taken into account, compared to earlier model versions where all surface meltwater was assumed to refreeze at the end of summer. The surface mass balance of ice sheet and ice shelf are now treated consistently with the same positive-degree-day model including capillary water and refreezing terms. The same melting schemes for basal and surface melt have been used for the AIS model version that participated in the PlioMIP intercomparison exercise of de Boer et al. (2015).

The atmospheric interface for the GrIS was redesigned to enable ice sheet regrowth from a (semi-) deglaciated state given favourable conditions. This is accomplished by calculating surface temperatures independently for different surface types (ocean, ice sheet, tundra), which most importantly prevents tundra warming to affect proximal ice sheet margins. At the same time, the full range of atmospheric forcing is taken into account by allowing the ice sheet forcing temperature to exceed the melting point at the surface. This provides an in principle unbounded temperature anomaly forcing for increasing atmospheric heat content for the positive-degree-day melt scheme.

10 References

Bamber, J. L., Riva, R. E. M., Vermeersen, B. L. A., and LeBrocq, A. M.: Reassessment of the Potential Sea-Level Rise from a Collapse of the West Antarctic Ice Sheet, Science, 324, 901-903, doi:10.1126/science.1169335, 2009.

Beckmann, A., and Goosse, H.: A parameterization of ice shelf-ocean interaction for climate models, Ocean Modell., 5, 157-170, doi:10.1016/S1463-5003(02)00019-7, 2003.

768   Berger, A.: Long-term variations of daily insolation and Quaternary climatic changes, Journal

769   of Atmospheric Sciences, 35, 2362-2367, doi:10.1175/1520-

770   0469(1978)035<2362:LTVODI>2.0.CO;2, 1978.

771   Bianchi, C., and Gersonde, R.: The Southern Ocean surface between Marine Isotope Stages 6

772   and 5d: Shape and timing of climate changes, Palaeogeography, Palaeoclimatology,

773   Palaeoecology, 187, 151-177, doi:10.1016/S0031-0182(02)00516-3, 2002.

774   Born, A., and Nisancioglu, K. H.: Melting of Northern Greenland during the last

775   interglaciation, Cryosphere, 6, 1239-1250, doi:10.5194/tc-6-1239-2012, 2012.

776   Brovkin, V., Ganopolski, A., and Svirezhev, Y.: A continuous climate-vegetation

777   classification for use in climate-biosphere studies, Ecol. Model., 101, 251-261,

778   doi:10.1016/S0304-3800(97)00049-5, 1997.

779   Calov, R., Robinson, A., Perrette, M., and Ganopolski, A.: Simulating the Greenland ice sheet

780   under present-day and palaeo constraints including a new discharge parameterization, The

781   Cryosphere, 9, 179-196, doi:10.5194/tc-9-179-2015, 2015.

782   Capron, E., Govin, A., Stone, E. J., Masson-Delmotte, V., Mulitza, S., Otto-Bliesner, B.,

783   Rasmussen, T. L., Sime, L. C., Waelbroeck, C., and Wolff, E. W.: Temporal and spatial

784   structure of multi-millennial temperature changes at high latitudes during the Last

785   Interglacial, Quat. Sci. Rev., 103, 116-133, doi:10.1016/j.quascirev.2014.08.018, 2014.

786   Clark, P., Marshall, S., Clarke, G., Hostetler, S., Licciardi, J., and Teller, J.: Freshwater

787   forcing of abrupt climate change during the last glaciation, Science, 293, 283-287,

788   doi:10.1126/science.1062517, 2001.

789   CLIMAP project members: Seasonal reconstruction of the earth's surface at the last glacial

790   maximum, Geol.Soc.Am.Map Chart Ser., MC-36, 1981.

791   Colville, E. J., Carlson, A. E., Beard, B. L., Hatfield, R. G., Stoner, J. S., Reyes, A. V., and

792   Ullman, D. J.: Sr-Nd-Pb Isotope Evidence for Ice-Sheet Presence on Southern Greenland

793   During the Last Interglacial, Science, 333, 620-623, doi:10.1126/science.1204673, 2011.

794   Dansgaard, W., Clausen, H. B., Gundestrup, N., Hammer, C. U., Johnsen, S. F., Kristinsdottir,

795   P. M., and Reeh, N.: A New Greenland Deep Ice Core, Science, 218, 1273-1277,

796   doi:10.1126/science.218.4579.1273, 1982.

797   de Boer, B., van de Wal, R. S. W., Lourens, L. J., Bintanja, R., and Reerink, T. J.: A

798   continuous simulation of global ice volume over the past 1 million years with 3-D ice-sheet

799   models, Clim. Dyn., 41, 1365-1384, doi:10.1007/s00382-012-1562-2, 2013.

800   de Boer, B., Stocchi, P., and van de Wal, R. S. W.: A fully coupled 3-D ice-sheet-sea-level

801   model: algorithm and applications, Geosci. Model Dev., 7, 2141-2156, doi:10.5194/gmd-7-

802   2141-2014, 2014.

803   de Boer, B., Dolan, A. M., Bernales, J., Gasson, E., Goelzer, H., Golledge, N. R., Sutter, J.,

804   Huybrechts, P., Lohmann, G., Rogozhina, I., Abe-Ouchi, A., Saito, F., and van de Wal, R. S.

805   W.: Simulating the Antarctic ice sheet in the late-Pliocene warm period: PLISMIP-ANT, an

806   ice-sheet model intercomparison project, The Cryosphere, 9, 881-903, doi:10.5194/tc-9-881-

807   2015, 2015.

808   DeConto, R. M., and Pollard, D.: Contribution of Antarctica to past and future sea-level rise,

809   Nature, 531, 591-+, doi:10.1038/nature17145, 2016.

810   Depoorter, M. A., Bamber, J. L., Griggs, J. A., Lenaerts, J. T. M., Ligtenberg, S. R. M., van

811   den Broeke, M. R., and Moholdt, G.: Calving fluxes and basal melt rates of Antarctic ice

812   shelves, Nature, 502, 89-+, doi:10.1038/nature12567, 2013.

813   Driesschaert, E., Fichefet, T., Goosse, H., Huybrechts, P., Janssens, I., Mouchet, A.,

814   Munhoven, G., Brovkin, V., and Weber, S.: Modeling the influence of Greenland ice sheet

815   melting on the Atlantic meridional overturning circulation during the next millennia,

816   Geophys. Res. Lett., 34, 10707, doi:10.1029/2007GL029516, 2007.

817   Duplessy, J. C., Roche, D. M., and Kageyama, M.: The deep ocean during the last interglacial

818   period, Science, 316, 89-91, doi:10.1126/science.1138582, 2007.

819   Dutton, A., Carlson, A. E., Long, A. J., Milne, G. A., Clark, P. U., DeConto, R., Horton, B.

820   P., Rahmstorf, S., and Raymo, M. E.: Sea-level rise due to polar ice-sheet mass loss during

821   past warm periods, Science, 349, doi:10.1126/science.aaa4019, 2015.

822   Dutton, A., and Lambeck, K.: Ice Volume and Sea Level During the Last Interglacial,

823   Science, 337, 216-219, doi:10.1126/science.1205749, 2012.

824   EPICA community members: Eight glacial cycles from an Antarctic ice core, Nature, 429,

825   623-628, doi:10.1038/Nature02599, 2004.

826 Fretwell, P., Pritchard, H. D., Vaughan, D. G., Bamber, J. L., Barrand, N. E., Bell, R.,
827 Bianchi, C., Bingham, R. G., Blankenship, D. D., Casassa, G., Catania, G., Callens, D.,
828 Conway, H., Cook, A. J., Corr, H. F. J., Damaske, D., Damm, V., Ferraccioli, F., Forsberg,
829 R., Fujita, S., Gim, Y., Gogineni, P., Griggs, J. A., Hindmarsh, R. C. A., Holmlund, P., Holt,
830 J. W., Jacobel, R. W., Jenkins, A., Jokat, W., Jordan, T., King, E. C., Kohler, J., Krabill, W.,
831 Riger-Kusk, M., Langley, K. A., Leitchenkov, G., Leuschen, C., Luyendyk, B. P., Matsuoka,
832 K., Mouginot, J., Nitsche, F. O., Nogi, Y., Nost, O. A., Popov, S. V., Rignot, E., Rippin, D.
833 M., Rivera, A., Roberts, J., Ross, N., Siegert, M. J., Smith, A. M., Steinhage, D., Studinger,
834 M., Sun, B., Tinto, B. K., Welch, B. C., Wilson, D., Young, D. A., Xiangbin, C., and
835 Zirizzotti, A.: Bedmap2: improved ice bed, surface and thickness datasets for Antarctica,
836 Cryosphere, 7, 375-393, doi:10.5194/tc-7-375-2013, 2013.

837 Fürst, J. J., Goelzer, H., and Huybrechts, P.: Effect of higher-order stress gradients on the
838 centennial mass evolution of the Greenland ice sheet, The Cryosphere, 7, 183-199,
839 doi:10.5194/tc-7-183-2013, 2013.

840 Goelzer, H., Huybrechts, P., Loutre, M. F., Goosse, H., Fichefet, T., and Mouchet, A.: Impact
841 of Greenland and Antarctic ice sheet interactions on climate sensitivity, Clim. Dyn., 37, 1005-
842 1018, doi:10.1007/s00382-010-0885-0, 2011.

843 Goelzer, H., Huybrechts, P., Raper, S. C. B., Loutre, M. F., Goosse, H., and Fichefet, T.:
844 Millennial total sea level commitments projected with the Earth system model of intermediate
845 complexity LOVECLIM Environ. Res. Lett., 7, 045401, doi:10.1088/1748-9326/7/4/045401,
846 2012.

847 Goelzer, H., Huybrechts, P., Loutre, M. F., and Fichefet, T.: Impact of ice sheet meltwater
848 fluxes on the climate evolution at the onset of the Last Interglacial, Clim. Past. Discuss., 11,
849 4391-4423, doi:10.5194/cpd-11-4391-2015, 2016.

850 Golledge, N. R., Menviel, L., Carter, L., Fogwill, C. J., England, M. H., Cortese, G., and
851 Levy, R. H.: Antarctic contribution to meltwater pulse 1A from reduced Southern Ocean
852 overturning, Nature Communications, 5, 5107, doi:10.1038/ncomms6107, 2014.

853 Goosse, H., Brovkin, V., Fichefet, T., Haarsma, R., Huybrechts, P., Jongma, J., Mouchet, A.,
854 Selten, F., Barriat, P.-Y., Campin, J.-M., Deleersnijder, E., Driesschaert, E., Goelzer, H.,
855 Janssens, I., Loutre, M. F., Morales Maqueda, M. A., Opsteegh, T., Mathieu, P.-P.,
856 Munhoven, G., Pettersson, E. J., Renssen, H., Roche, D. M., Schaeffer, M., Tartinville, B.,

857 Timmermann, A., and Weber, S. L.: Description of the Earth system model of intermediate

858 complexity LOVECLIM version 1.2, Geosci. Model Dev., 3, 603-633, doi:10.5194/gmd-3-

859 603-2010, 2010.

860 Goosse, H., and Fichefet, T.: Importance of ice-ocean interactions for the global ocean

861 circulation: A model study, J. Geophys. Res., 104, 23337-23355, doi:10.1029/1999JC900215,

862 1999.

863 Grant, K. M., Rohling, E. J., Bar-Matthews, M., Ayalon, A., Medina-Elizalde, M., Ramsey,

864 C. B., Satow, C., and Roberts, A. P.: Rapid coupling between ice volume and polar

865 temperature over the past 150,000 years, Nature, 491, 744–747, doi:10.1038/nature11593,

866 2012.

867 Helsen, M. M., van de Berg, W. J., van de Wal, R. S. W., van den Broeke, M. R., and

868 Oerlemans, J.: Coupled regional climate-ice-sheet simulation shows limited Greenland ice

869 loss during the Eemian, Clim. Past., 9, 1773-1788, doi:10.5194/cp-9-1773-2013, 2013.

870 Holden, P., Edwards, N. R., Wolff, E., Lang, N., Singarayer, J., Valdes, P., and Stocker, T.:

871 Interhemispheric coupling, the West Antarctic Ice Sheet and warm Antarctic interglacials,

872 Clim. Past., 6, 431-443, doi:10.5194/cp-6-431-2010, 2010.

873 Huybrechts, P.: Sea-level changes at the LGM from ice-dynamic reconstructions of the

874 Greenland and Antarctic ice sheets during the glacial cycles, Quat. Sci. Rev., 21, 203-231,

875 doi:10.1016/S0277-3791(01)00082-8, 2002.

876 Huybrechts, P., and de Wolde, J.: The dynamic response of the Greenland and Antarctic ice

877 sheets to multiple-century climatic warming, J. Clim., 12, 2169-2188, doi:10.1175/1520-

878 0442(1999)012<2169:TDROTG>2.0.CO;2, 1999.

879 Huybrechts, P., Goelzer, H., Janssens, I., Driesschaert, E., Fichefet, T., Goosse, H., and

880 Loutre, M. F.: Response of the Greenland and Antarctic Ice Sheets to Multi-Millennial

881 Greenhouse Warming in the Earth System Model of Intermediate Complexity LOVECLIM,

882 Surv. Geophys., 32, 397-416, doi:10.1007/s10712-011-9131-5, 2011.

883 Janssens, I., and Huybrechts, P.: The treatment of meltwater retention in mass-balance

884 parameterizations of the Greenland ice sheet, Ann. Glaciol., 31, 133-140, 2000.

885   Kopp, R. E., Simons, F. J., Mitrovica, J. X., Maloof, A. C., and Oppenheimer, M.:
886   Probabilistic assessment of sea level during the last interglacial stage, Nature, 462, 863-867,
887   doi:10.1038/nature08686, 2009.

888   Kopp, R. E., Simons, F. J., Mitrovica, J. X., Maloof, A. C., and Oppenheimer, M.: A
889   probabilistic assessment of sea level variations within the last interglacial stage, Geophys. J.
890   Int., 193, 711-716, doi:10.1093/gji/ggt029, 2013.

891   Landais, A., Masson-Delmotte, V., Capron, E., Langebroek, P. M., Bakker, P., Stone, E. J.,
892   Merz, N., Raible, C. C., Fischer, H., Orsi, A., Prié, F., Vinther, B., and Dahl-Jensen, D.: How
893   warm was Greenland during the last interglacial period?, Clim. Past Discuss., 2016, 1-27,
894   doi:10.5194/cp-2016-28, 2016.

895   Langebroek, P. M., and Nisancioglu, K. H.: Moderate Greenland ice sheet melt during the last
896   interglacial constrained by present-day observations and paleo ice core reconstructions, The
897   Cryosphere Discuss., 2016, 1-35, doi:10.5194/tc-2016-15, 2016.

898   Lisiecki, L. E., and Raymo, M. E.: A Pliocene-Pleistocene stack of 57 globally distributed
899   benthic delta O-18 records, Paleoceanography, 20, PA1003, doi:10.1029/2004pa001071,
900   2005.

901   Loutre, M. F., Fichefet, T., Goosse, H., Huybrechts, P., Goelzer, H., and Capron, E.: Factors
902   controlling the last interglacial climate as simulated by LOVECLIM1.3, Clim. Past., 10,
903   1541-1565, doi:10.5194/cp-10-1541-2014, 2014.

904   MacGregor, J. A., and Fahnestock, M. A.: Radiostratigraphy and age structure of the
905   Greenland Ice Sheet, J Geophys Res-Earth, 120, 212–241, doi:10.1002/2014JF003215, 2015.

906   Masson-Delmotte, V., Schulz, M., Abe-Ouchi, A., Beer, J., Ganopolski, A., González Rouco,
907   J., Jansen, E., Lambeck, K., Luterbacher, J., Naish, T., Osborn, T., Otto-Bliesner, B., Quinn,
908   T., Ramesh, R., Rojas, M., Shao, X., and Timmermann, A.: Information from paleoclimate
909   archives, in: Climate Change 2013: The Physical Science Basis. Contribution of Working
910   Group I to the Fifth Assessment Report of the Intergovernmental Panel on Climate Change,
911   edited by: Stocker, T. F., Qin, D., Plattner, G.-K., Tignor, M., Allen, S. K., Boschung, J.,
912   Nauels, A., Xia, Y., Bex, V., and Midgley, P. M., Cambridge University Press, Cambridge,
913   United Kingdom and New York, NY, USA, 383-464, 2013.

914   Masson-Delmotte, V., Steen-Larsen, H. C., Ortega, P., Swingedouw, D., Popp, T., Vinther, B.
915   M., Oerter, H., Sveinbjornsdottir, A. E., Gudlaugsdottir, H., Box, J. E., Falourd, S., Fettweis,

916 X., Gallee, H., Garnier, E., Gkinis, V., Jouzel, J., Landais, A., Minster, B., Paradis, N., Orsi,
917 A., Risi, C., Werner, M., and White, J. W. C.: Recent changes in north-west Greenland
918 climate documented by NEEM shallow ice core data and simulations, and implications for
919 past-temperature reconstructions, Cryosphere, 9, 1481-1504, doi:10.5194/tc-9-1481-2015,
920 2015.

921 Mckay, N. P., Overpeck, J. T., and Otto-Bliesner, B. L.: The role of ocean thermal expansion
922 in Last Interglacial sea level rise, Geophys. Res. Lett., 38, L14605,
923 doi:10.1029/2011GL048280, 2011.

924 Menviel, L., Spence, P., and England, M. H.: Contribution of enhanced Antarctic Bottom
925 Water formation to Antarctic warm events and millennial-scale atmospheric CO2 increase,
926 Earth Planet. Sci. Lett., 413, 37-50, doi:10.1016/j.epsl.2014.12.050, 2015.

927 Merz, N., Born, A., Raible, C. C., Fischer, H., and Stocker, T. F.: Dependence of Eemian
928 Greenland temperature reconstructions on the ice sheet topography, Clim. Past, 10, 1221-
929 1238, doi:10.5194/cp-10-1221-2014, 2014.

930 Merz, N., Born, A., Raible, C. C., and Stocker, T. F.: Warm Greenland during the last
931 interglacial: the role of regional changes in sea ice cover, Clim. Past Discuss., 2016, 1-37,
932 doi:10.5194/cp-2016-12, 2016.

933 NEEM community members: Eemian interglacial reconstructed from a Greenland folded ice
934 core, Nature, 493, 489-494, doi:10.1038/nature11789, 2013.

935 Nowicki, S. M. J., Payne, T., Larour, E., Seroussi, H., Goelzer, H., Lipscomb, W., Gregory,
936 J., Abe-Ouchi, A., and Shepherd, A.: Ice Sheet Model Intercomparison Project (ISMIP6)
937 contribution to CMIP6, Geosci. Model Dev. Discuss., 2016, 1-42, doi:10.5194/gmd-2016-
938 105, 2016.

939 Opsteegh, J. D., Haarsma, R. J., Selten, F. M., and Kattenberg, A.: ECBILT: a dynamic
940 alternative to mixed boundary conditions in ocean models, Tellus, 50, 348-367,
941 doi:10.1034/j.1600-0870.1998.t01-1-00007.x, 1998.

942 Pedersen, R. A., Langen, P. L., and Vinther, B. M.: Greenland warming during the last
943 interglacial: the relative importance of insolation and oceanic changes, Clim. Past Discuss.,
944 2016, 1-20, doi:10.5194/cp-2016-48, 2016.

945 Pollard, D., and DeConto, R. M.: Modelling West Antarctic ice sheet growth and collapse
946 through the past five million years, Nature, 458, 329-332, doi:10.1038/nature07809, 2009.

947 Pollard, D., DeConto, R. M., and Alley, R. B.: Potential Antarctic Ice Sheet retreat driven by
948 hydrofracturing and ice cliff failure, Earth Planet. Sci. Lett., 412, 112-121,
949 doi:10.1016/j.epsl.2014.12.035, 2015.

950 Robinson, A., Calov, R., and Ganopolski, A.: Greenland ice sheet model parameters
951 constrained using simulations of the Eemian Interglacial, Clim. Past., 7, 381-396,
952 doi:10.5194/cp-7-381-2011, 2011.

953 Robinson, A., and Goelzer, H.: The importance of insolation changes for paleo ice sheet
954 modeling, The Cryosphere, 8, 1419-1428, doi:10.5194/tc-8-1419-2014, 2014.

955 Rohling, E. J., Foster, G. L., Grant, K. M., Marino, G., Roberts, A. P., Tamisiea, M. E., and
956 Williams, F.: Sea-level and deep-sea-temperature variability over the past 5.3 million years,
957 Nature, 508, 477–482, doi:10.1038/nature13230, 2014.

958 Shakun, J. D., Lea, D. W., Lisiecki, L. E., and Raymo, M. E.: An 800-kyr record of global
959 surface ocean delta O-18 and implications for ice volume-temperature coupling, Earth Planet.
960 Sci. Lett., 426, 58-68, doi:10.1016/j.epsl.2015.05.042, 2015.

961 Sjolte, J., and Hoffmann, G.: Modelling stable water isotopes in monsoon precipitation during
962 the previous interglacial, Quat. Sci. Rev., 85, 119-135, doi:10.1016/j.quascirev.2013.12.006,
963 2014.

964 Steen-Larsen, H. C., Masson-Delmotte, V., Hirabayashi, M., Winkler, R., Satow, K., Prié, F.,
965 Bayou, N., Brun, E., Cuffey, K. M., Dahl-Jensen, D., Dumont, M., Guillevic, M., Kipfstuhl,
966 S., Landais, A., Popp, T., Risi, C., Steffen, K., Stenni, B., and Sveinbjörnsdottír, A. E.: What
967 controls the isotopic composition of Greenland surface snow?, Clim. Past., 10, 377-392,
968 doi:10.5194/cp-10-377-2014, 2014.

969 Steig, E. J., Huybers, K., Singh, H. A., Steiger, N. J., Ding, Q. H., Frierson, D. M. W., Popp,
970 T., and White, J. W. C.: Influence of West Antarctic Ice Sheet collapse on Antarctic surface
971 climate, Geophys. Res. Lett., 42, 4862-4868, doi:10.1002/2015GL063861, 2015.

972 Stocker, T. F.: The Seesaw Effect, Science, 282, 61-62, doi:10.1126/science.282.5386.61,
973 1998.

974 Stone, E. J., Lunt, D. J., Annan, J. D., and Hargreaves, J. C.: Quantification of the Greenland
975 ice sheet contribution to Last Interglacial sea level rise, Clim. Past., 9, 621-639,
976 doi:10.5194/cp-9-621-2013, 2013.

977 Swingedouw, D., Fichefet, T., Huybrechts, P., Goosse, H., Driesschaert, E., and Loutre, M.
978 F.: Antarctic ice-sheet melting provides negative feedbacks on future climate warming,
979 Geophys. Res. Lett., 35, L17705, doi:10.1029/2008GL034410, 2008.

980 Thompson, W. G., Curran, H. A., Wilson, M. A., and White, B.: Sea-level oscillations during
981 the last interglacial highstand recorded by Bahamas corals, Nat. Geosci., 4, 684-687,
982 doi:10.1038/ngeo1253, 2011.

983 Turney, C. S. M., and Jones, R. T.: Does the Agulhas Current amplify global temperatures
984 during super-interglacials?, J. Quat. Sci., 25, 839-843, doi:10.1002/jqs.1423, 2010.

985 van de Berg, W. J., van den Broeke, M., Ettema, J., van Meijgaard, E., and Kaspar, F.:
986 Significant contribution of insolation to Eemian melting of the Greenland ice sheet, Nat.
987 Geosci., 4, 1-5, doi:10.1038/ngeo1245, 2011.

988 van de Berg, W. J., van den Broeke, M. R., van Meijgaard, E., and Kaspar, F.: Importance of
989 precipitation seasonality for the interpretation of Eemian ice core isotope records from
990 Greenland, Clim. Past., 9, 1589-1600, doi:10.5194/cp-9-1589-2013, 2013.

991 Vernon, C. L., Bamber, J. L., Box, J. E., Van Den Broeke, M. R., Fettweis, X., Hanna, E., and
992 Huybrechts, P.: Surface mass balance model intercomparison for the Greenland ice sheet, The
993 Cryosphere, 7, 599-614, doi:10.5194/tc-7-599-2013, 2013.

994 Yau, A. M., Bender, M. L., Robinson, A. and Brook, E. J.: Reconstructing the last interglacial
995 at Summit, Greenland: Insights from GISP2, Proceedings of the National Academy of
996 Sciences, 113(35), 9710–9715, doi:10.1073/pnas.1524766113, 2016.

997 Zweck, C., and Huybrechts, P.: Modeling of the northern hemisphere ice sheets during the
998 last glacial cycle and glaciological sensitivity, J. Geophys. Res, 110, D07103,
999 doi:10.1029/2004JD005489, 2005.

1000
1001

11 Tables

Table 1. Overview of all discussed model experiments. The second column gives the scale factor R for

temperature anomalies over the Greenland ice sheet.

Name	R	Description
Reference	0.4	Fully coupled reference simulation
High	0.5	Fully coupled simulation
Low	0.3	Fully coupled simulation
Forced reference	0.4	Forced with climate output from Reference
Forced high	0.5	Forced with climate output from Reference
Forced low	0.3	Forced with climate output from Reference
No sub-shelf melting	0.4	Suppressed Antarctic sub-shelf melting

1005

Table 2. Peak sea-level contribution in sea-level equivalent (SLE) and timing from the Greenland ice sheet

above present-day levels for three different parameter choices.

	Fully coupled experiments		Forced repeat experiments	
Name	SLE (m)	time of peak (kyr BP)	SLE (m)	time of peak (kyr BP)
High	+2.72	122.8	+2.01	123.6
Reference	+1.42	123.3	+1.42	123.3
Low	+0.65	124.0	+0.81	123.7

1008

1009

34

12 Figures
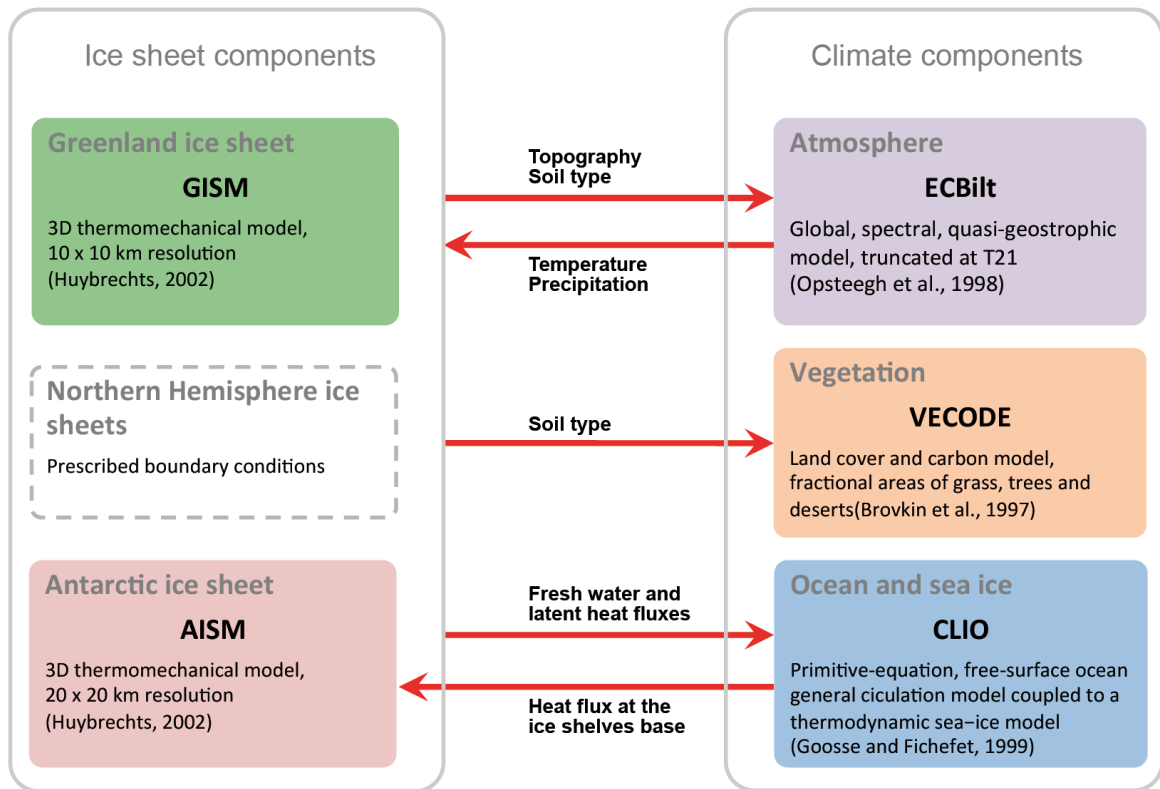
Fig. 1. LOVECLIM model setup for the present study including dynamic components for the Greenland and Antarctic ice sheets and prescribed Northern Hemisphere ice sheet boundary conditions.
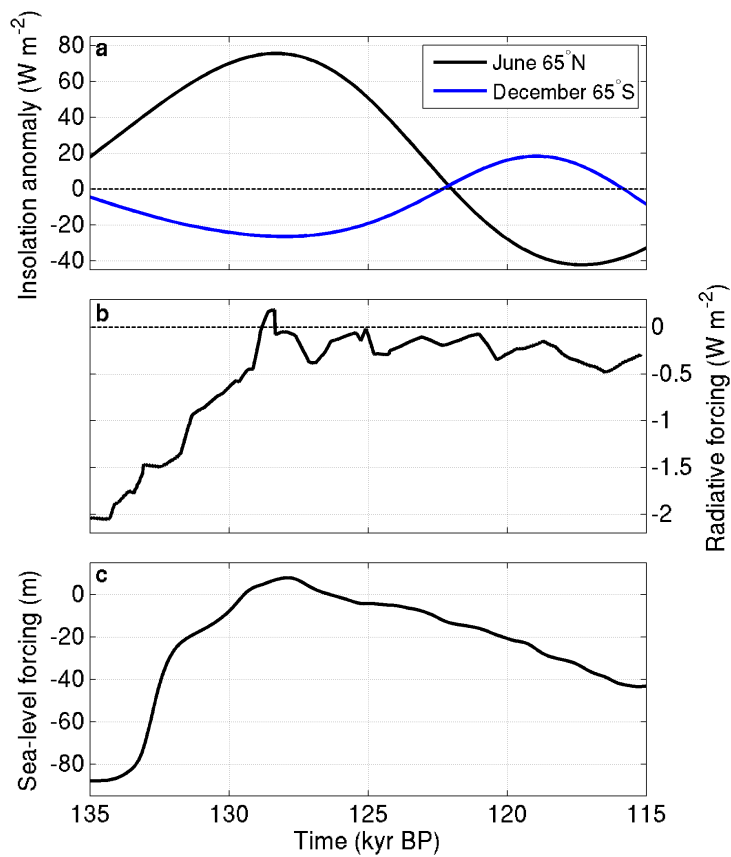
1016

1017   **Fig. 2. Prescribed model forcing. Average monthly insolation anomaly (a) at 65° North in June (black) and**
1018   **65° South in December (blue) to illustrate the spatially and temporally resolved forcing (Berger, 1978),**
1019   **combined radiative forcing anomaly of prescribed greenhouse gas concentrations relative to the present**
1020   **day (b) and sea-level forcing for the ice sheet components (c) derived from a Red Sea sea-level record**
1021   **(Grant et al. 2012).**

1022

1023
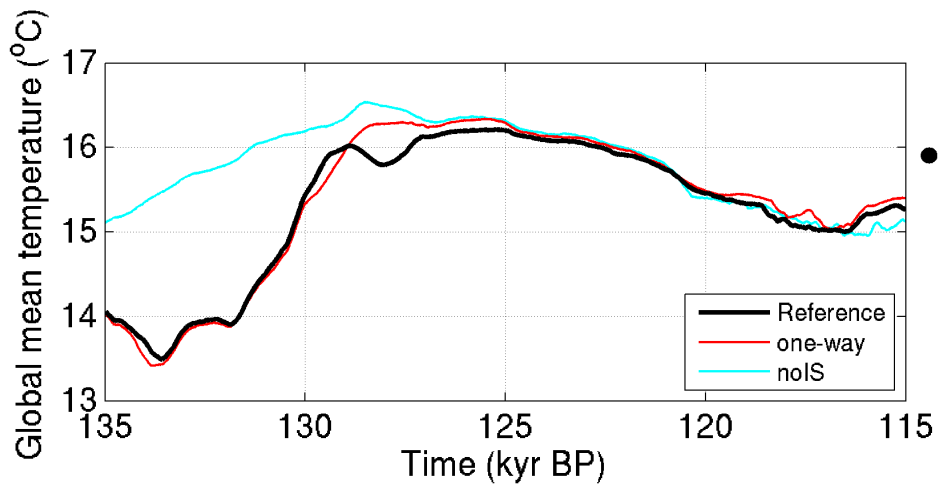
Fig. 3. Global annual mean near-surface air temperature evolution of the reference run (black) compared to experiments with prescribed Greenland and Antarctic ice sheet evolution from stand-alone experiments (One-way, red) and no ice sheet changes at all (noIS, light blue). The filled circle on the right axis indicates the temperature for a pre-industrial control experiment of the reference model with present-day ice sheet configuration.
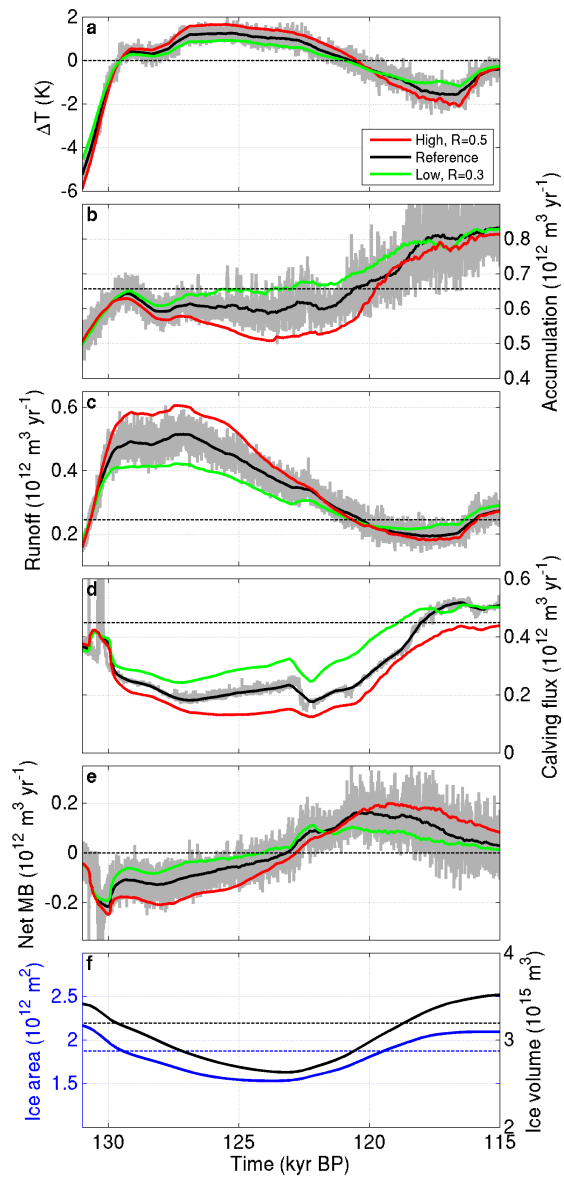
1033 **Fig. 4. Greenland ice sheet forcing characteristics for the reference run (black) and with higher (red) and**
1034 **lower (green) temperature scaling. Climatic temperature anomaly relative to pre-industrial (a).**
1035 **Accumulation (b) and surface meltwater runoff (c) over grounded ice. Calving flux (d), net mass balance**
1036 **(e) and other mass balance terms (b, c) given in water equivalent. Ice area (blue) and ice volume (black)**
1037 **for the reference run (f). All lines are smoothed with a 400 years running mean except for the grey lines**
1038 **giving the full annual time resolution for the reference run. Horizontal dashed lines give the pre-industrial**
1039 **reference values, except for panel e, where it is the zero line.**

1040
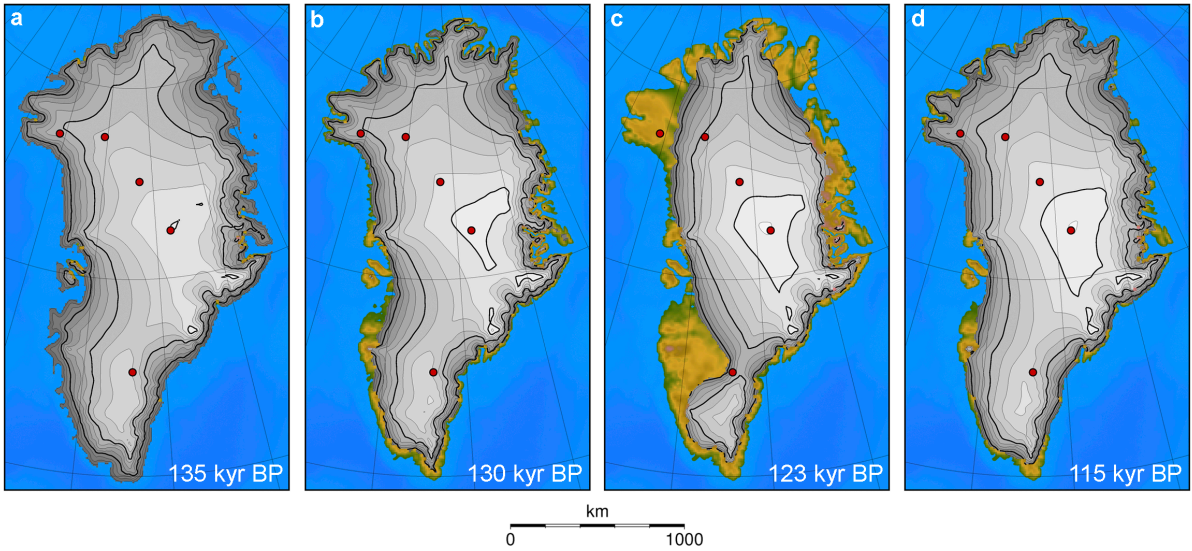
Fig. 5. Greenland ice sheet geometry at 135 kyr BP (a), 130 kyr BP (b), for the minimum ice sheet volume at 123 kyr BP with a sea-level contribution of 1.4 m (c) and at the end of the reference experiment at 115 kyr BP (d). The red dots indicate the deep ice core locations (from south to northwest: Dye-3, GRIP, NGRIP, NEEM, Camp Century).
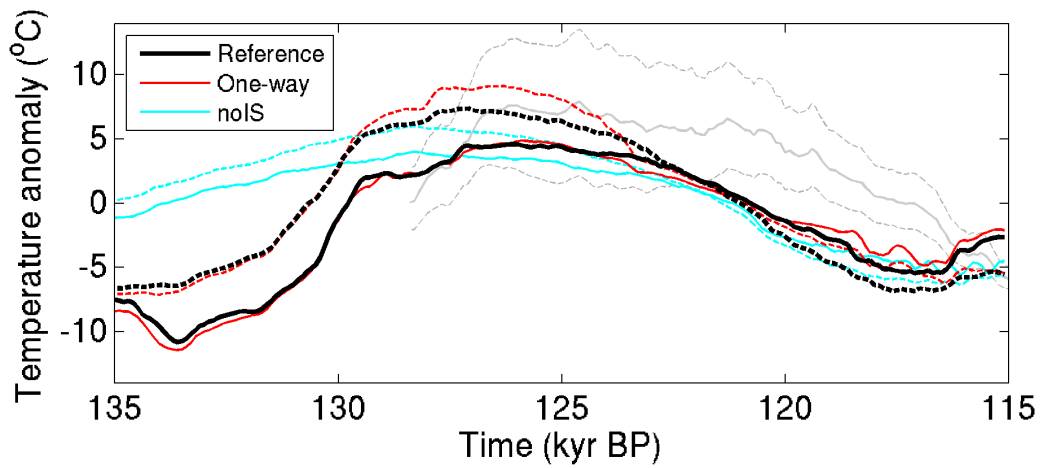
1048

1049 **Fig. 6. Comparison of modelled North-East Greenland annual mean (solid) and summer (June-July-**
1050 **August, dashed) surface temperature evolution (72° - 83° N and 306°33' - 317° 48' E) with reconstructed**
1051 **temperature changes (grey) at deep ice core site NEEM (77°27' N, 308°56' E). The solid grey line is the**
1052 **central estimate and grey dashed lines give the estimated error range for NEEM (NEEM community**
1053 **members, 2013).**

1054

1055

a

b
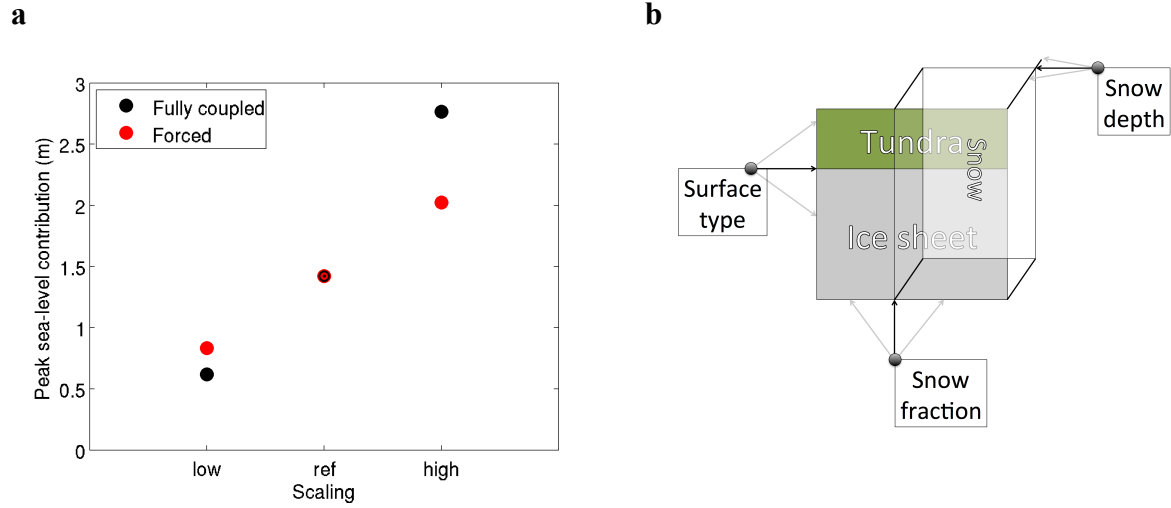
1056   **Fig. 7. Scaling of sea-level contribution from the Greenland ice sheet as a function of temperature changes**
1057   **for the full model (black) and forced model (red) in comparison (a). Schematic of the albedo**
1058   **parameterisation in the land model for (partially) ice-covered areas (b), which is a function of the**
1059   **underlying surface type, snow fraction and snow depth. See main text for details**
1060
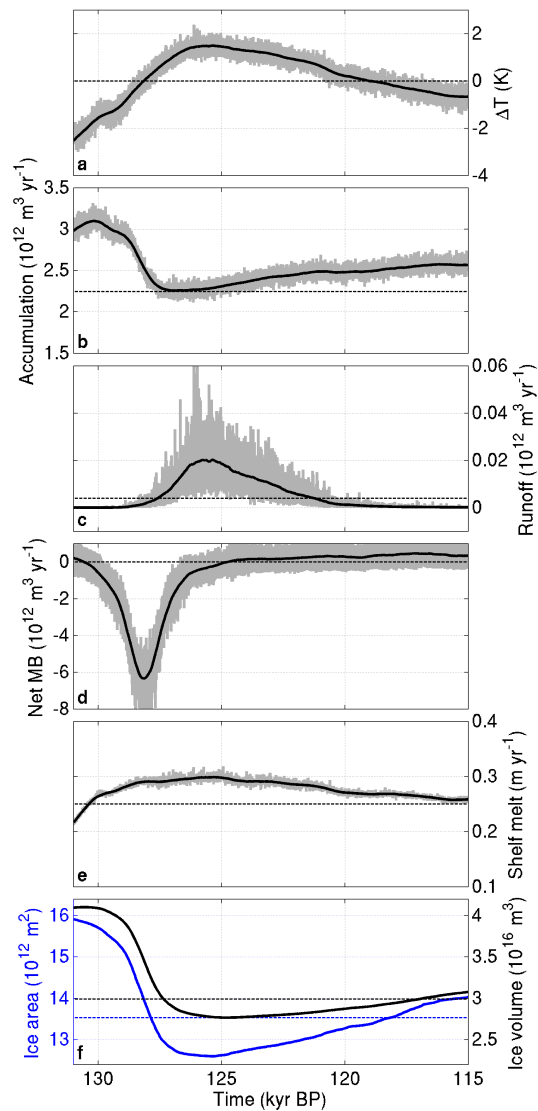
Fig. 8. Antarctic ice sheet forcing and characteristics. Temperature anomaly relative to pre-industrial (a), accumulation (b), surface meltwater runoff (c) and net mass balance of the grounded ice sheet (d), and average sub-shelf melt rate diagnosed for the area of the present-day observed ice shelves (e). Mass balance terms (b-e) are given in water equivalent. (f) Grounded ice sheet area (blue) and volume (black). Grey lines give full annual time resolution, while black lines (and blue in f) are smoothed with a 400 years running mean. Horizontal dashed lines give the pre-industrial reference values, except for panel d, where it is the zero line.
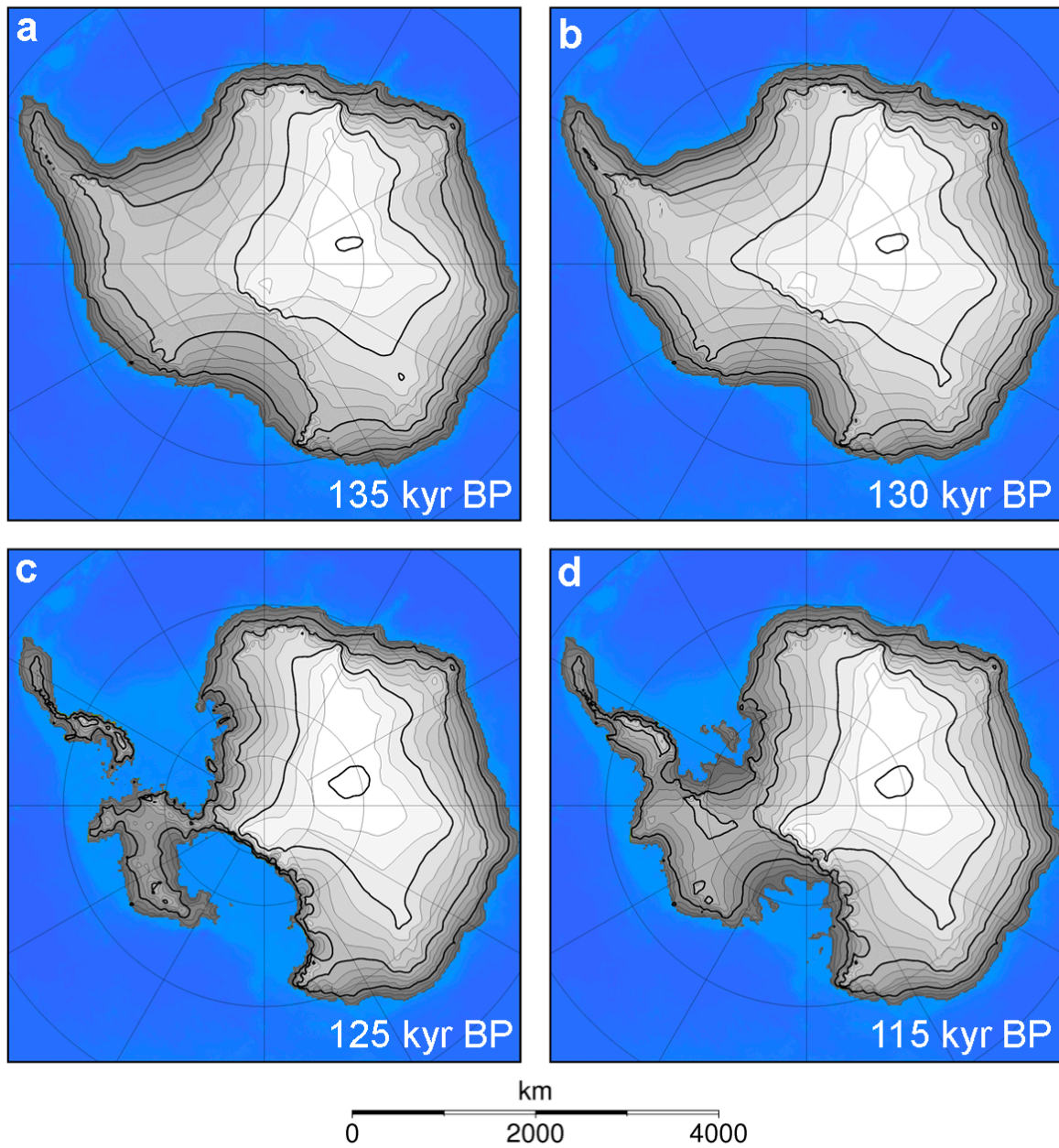
Fig. 9. Antarctic grounded ice sheet geometry at 135 kyr BP (a), 130 kyr BP (b), for the minimum ice sheet volume at 125 kyr BP with a sea-level contribution of 4.4 m (c) and at the end of the reference experiment at 115 kyr BP (d).
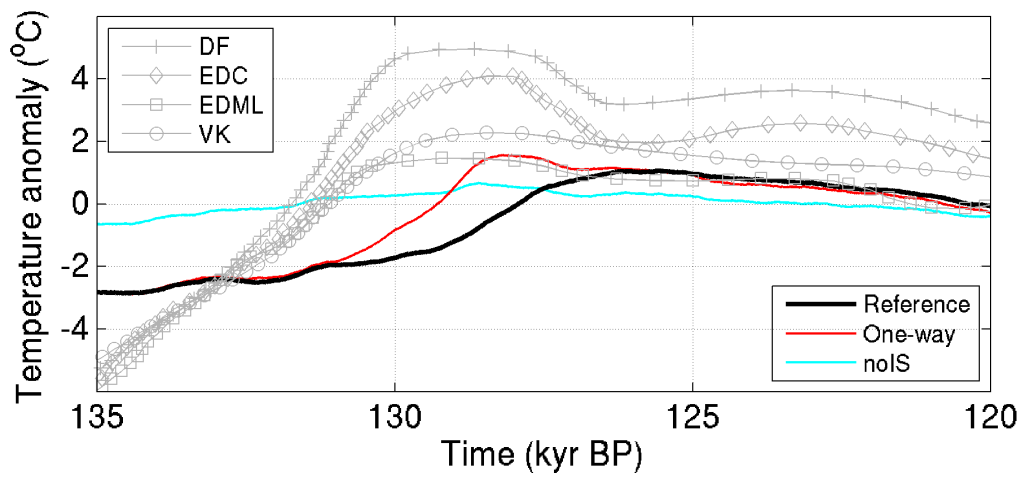
1076

Fig. 10. Comparison of modelled East Antarctic temperature evolution with reconstructed temperature changes at deep ice core sites. Modelled temperature anomalies are averaged over a region 72° - 90° S and 0° - 150° E. Ice core temperature reconstructions for the sites EPICA Dronning Maud Land (EDML, 75°00′ S, 00°04′ E), Dome Fuji (DF, 77°19′ S, 39°40′ E), Vostok (VK, 78°28′ S, 106°48′ E) and EPICA Dome C (EDC, 75°06′ S, 123°21′ E) are from Masson-Delmotte et al. (2011).

1082
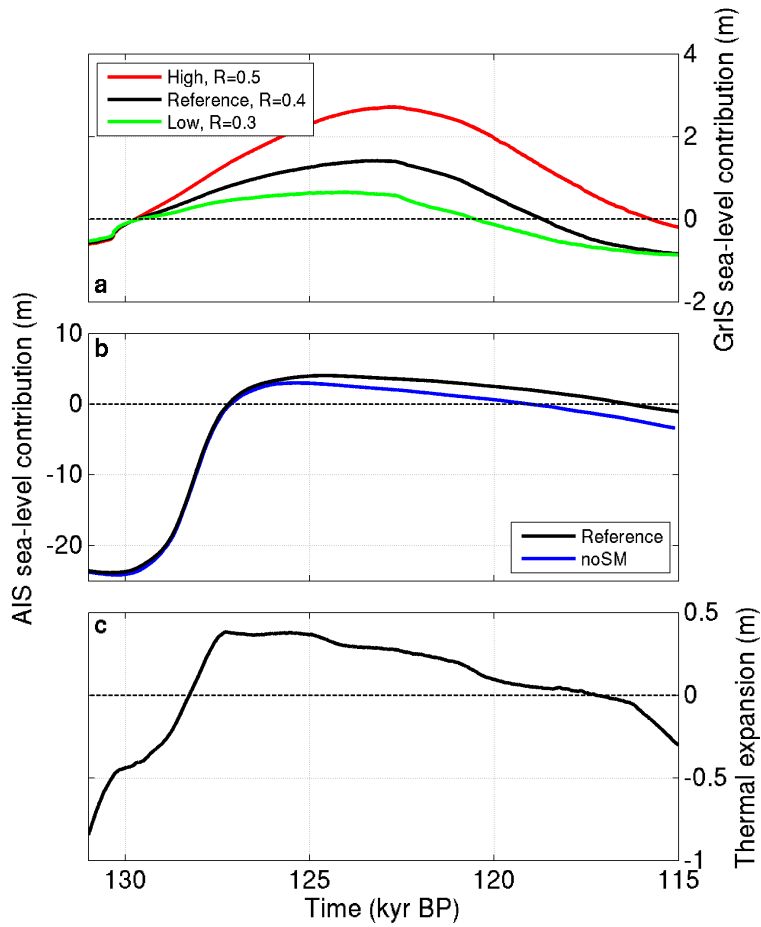
Fig. 11. Sea-level contribution from the Greenland ice sheet for the reference run (black) and two sensitivity experiments with higher (red) and lower (green) temperature scaling (a). Sea-level contribution from the Antarctic ice sheet (b) from the reference run (black) and from a sensitivity experiment without sub-shelf melting (blue). Sea-level contribution from oceanic thermal expansion from the reference run (c).

1090

1091
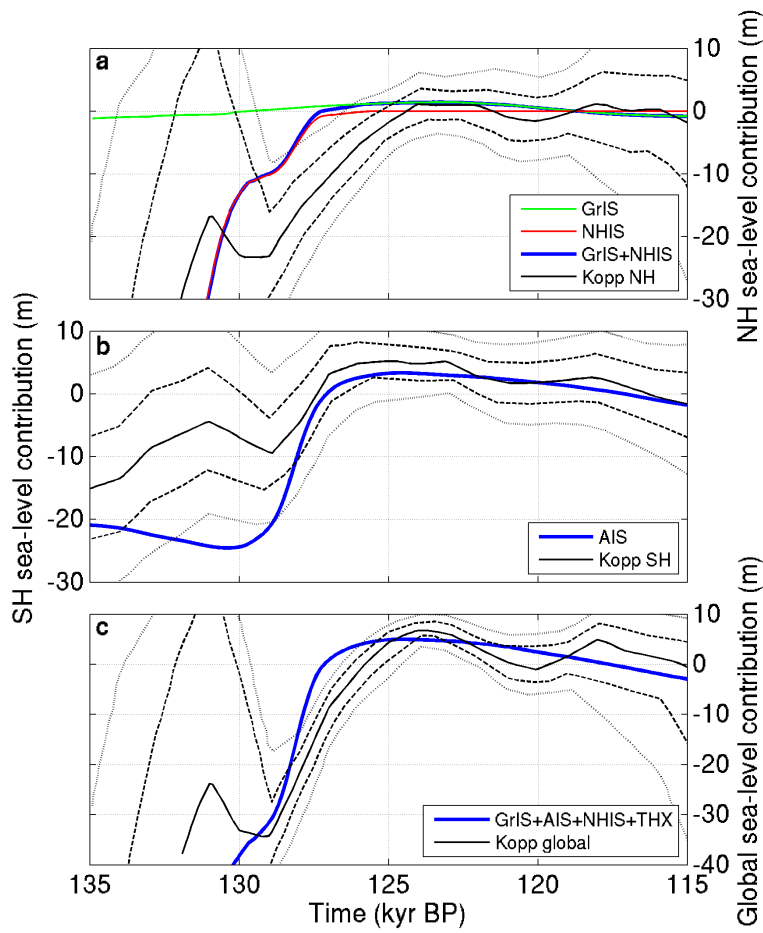
1092

Fig. 12. Modelled sea-level contributions from this study (colour lines) compared to probabilistic sea-level reconstructions (black lines) from Kopp et al. (2009) for the NH (a) the SH (b) and global (c). For the reconstructions, solid lines correspond to the median projection, dashed lines to the 16th and 84th percentiles, and dotted lines to the 2.5th and 97.5th percentiles.

1097